

The Attenuation of Very Cold Neutrons by Titanium Foil

By Philip Gabriel

C

A thesis submitted to the Faculty of Graduate Studies  
and Research in partial fulfillment of the requirements  
for the degree of Master of Science.

February 1981

## Table of Contents

Abstract .....	i
Preface .....	ii
Acknowledgements .....	iii

### Chapter One

Classification of Neutrons by energy .....	1
Thermal Neutrons .....	1
Slow Neutrons .....	2
Very Cold and Ultra Cold Neutrons .....	2
Interactions of Slow Neutrons with Matter .....	3
Types of Slow Neutron Scattering .....	9
Coherent and Incoherent Scattering .....	9
Incoherent Scattering .....	9
Inelastic Scattering .....	11
Inhomogeneous Elastic Scattering .....	13
Bragg Scattering .....	14
Total Reflection of Neutrons from Material Walls .....	15
Production of UCN .....	17

### Chapter Two- Experimental Procedure.....21

### Chapter Three- Analysis of Results.....27

Interpretation of the Attenuation Experiment.....	30
Sources of Error.....	35
Loss Mechanisms for UCN and VCN.....	39
Losses due to Impurities.....	40
Losses due to System Timing Errors.....	40

Conclusion.....	42
Table 1.....	44
Table 2.....	45
Table 3.....	46
Table 4.....	47
Figures and Captions.....	48
References .....	70

Abstract

Cross section measurements of titanium foil using neutrons having energies between  $10^{-6}$  -  $10^{-7}$  e.v. are presented. It is found that the experimental values for the sum of the nuclear absorption and the non nuclear inelastic cross sections are consistent with the '1/v' law.

## Sommaire

Des mesures de section efficace sur une feuille de titanium obtenus à l'aide de neutrons d'énergie comprise entre  $10^{-6}$ - $10^{-7}$  e.v. sont présentées. Les valeurs expérimentales de la somme de l'absorption nucléaire et des sections efficaces inélastiques non-nucléaires sont en accord avec la loi en  $1/v$ .

### Preface

This Thesis is the result of work performed at Chalk River and McGill University under the supervision of Professor J.M. Robson during the 1979-1980 academic year.

The experimental determination of the sum of the nuclear absorption and the non nuclear inelastic cross sections using extremely low energy neutrons is the subject of this thesis.

The physical importance of this measurement lies in the confirmation of the  $1/v$  law for neutrons approaching the zero energy asymptotic limit. The practical usefulness of this measurement is in connection with the design of windows for low energy neutron detector.

Acknowledgements

I would like to thank Dr. M.A. Lone and Mr. D. Tennant of the C.R.N.L for their invaluable assistance and advice in adjusting the electronic equipment. I also thank Dr. G. Dolling and Dr. W.L. Buyers for their interesting and helpful discussions concerning the interpretation of my data. Finally, but not the least, I wish to thank my director Professor John Robson for his patient and useful guidance during the time I took to perform the work presented here.

## Chapter One

In this section the nomenclature is introduced, and concepts to be discussed throughout this work will be described.

### Classification of Neutrons by Energy

In order to describe neutron interactions with matter it is useful to classify them according to their kinetic energy. It is possible to separate neutrons of a variety of energies into fairly definite groups. The divisions in general occur naturally as a result of the interactions peculiar to certain energy ranges.

### Thermal Neutrons

When fast neutrons have been slowed down until the average energy of the neutrons is equal to the average thermal energy of the atoms of the medium, the neutrons are called thermal neutrons. The energies and corresponding velocities of the neutrons then depend upon the temperature of the medium. Provided the medium does not contain strong neutron absorbers the velocity distribution can be approximated by the Maxwell distribution:

$$n(v)dv = 4\pi n_0 \left( \frac{m}{2\pi kT} \right)^{3/2} v^2 e^{-\frac{mv^2}{2kT}} dv \quad (1)$$

where  $v$  is the neutron velocity,  $m$  its mass,  $k$  is Boltzmann's constant and  $T$  the absolute temperature. The maximum of the velocity distribution occurs when the neutron energy is equal to  $kT$ . At  $20^\circ\text{C}$  the value of  $kT$  is about 25 milli-electron volts (mev), and the corresponding most probable neutron velocity is 2200 meters/second (m/sec).



### Slow Neutrons

Neutrons having energies from 0 to about  $10^3$  e.v are usually included in the category of slow neutrons. A number of subclassifications in this range occur. In addition to thermal neutrons, the two classifications which are of importance to this work are described below.

#### Very cold and Ultra cold Neutrons

It was Fermi who first deduced that the scattering of neutrons by individual nuclei means that neutrons propagating through matter would be refracted as light or x-rays and that neutrons incident on a surface at a glancing angle  $\theta_c$  which satisfies :

$$\sin \theta_c \leq (V/E)^{1/2} \quad (2)$$

will undergo total reflection, analogous to the phenomenon of total reflection in optics. In equation (2)  $V$  is of the order of  $10^{-7}$  ev and is a potential characteristic of the material and  $E$  is the neutron energy. The observation of this effect by Fermi and Zinn (1946) and Fermi and Marshall (1947) led some people to speculate that neutrons with an energy:

$$E \leq V \quad (3)$$

would suffer total reflection at any angle of incidence from a material surface and hence could be stored in bottles. Neutrons satisfying condition (3) are referred to as ultra cold neutrons (UCN), whereas neutrons violating (3) but satisfying (2) for glancing angles greater than a few degrees, (for a 100 m/sec neutron  $\theta_c$  is about  $3^\circ$ ) are termed very cold neutrons.

### Interactions of slow neutrons with matter

In order of decreasing strength, the interactions of slow neutrons with matter are: A) the nuclear interaction, B) the magnetic interaction C) the weak interaction and D) the gravitational interaction. Of these, only the nuclear interaction will be discussed as it is dominant and pertinent to the description of the experimental results described in this thesis.

The interaction of a slow neutron with another nucleon can be adequately described as a strong short range attraction. When a neutron interacts with a nucleus, the result of the attraction to individual nucleons can be characterized (for low neutron energies) as an attractive potential with a depth of about 40 Mev and a size slightly larger than the size of the nucleus, or a few times  $10^{-13}$  cms. With decreasing neutron energy, the scattering becomes predominantly S-wave i.e, isotropic in the center of mass, and independent of the attractive potential (Blatt and Weiskopff 1952). In fact at low enough energies, (including the energies with which we are concerned in this thesis), the scattering depends on a single parameter—the scattering length — which will be symbolized by the letter  $a$ . At low energies the scattering length is related to the S-wave phase shift through the relation:

$$\delta_s^0 = -ka \quad (4)$$

This equation relates the phase shift  $\delta_s$  to the scattering length and the reciprocal wavelength of the neutron denoted by  $k$ .

The significance of the scattering length can be established simply. At very low energies the wave function of the neutron outside the range of the potential can be expressed as a plane wave having the form:

$$\psi \propto \sin k(r-a) \approx k(r-a) \quad (5)$$

The scattering length is therefore the extrapolated intercept of the the wave function on the  $r$  axis as shown in fig 1. It is seen that if the inner wave function has a negative slope at  $r=r_0$ ,  $a$  is positive. Since a negative slope implies a possible bound state, scattering from a potential giving a bound state produces a positive  $a$ . Similarly if the potential gives only a virtual state, the slope of the inner wave function at  $r=r_0$  is positive and  $a$  is negative.

A positive scattering length may be compared to the range of interaction of a spherical potential. This potential can be approximated by an impermeable, or infinitely hard sphere. The incoming and outgoing waves are in this instance  $180^\circ$  out of phase with one another and exhibit destructive interference. If one could produce a potential that allowed for a zero phase shift between the incident and outgoing waves, then constructive interference would result and the potential barrier would be permeable. This situation is illustrated in fig 2.

The wave function describing the scattering may be expressed as a superposition of an incoming plane wave and an outgoing spherical wave:

$$\psi = e^{ik \cdot r} + \{f(\theta)/r\} e^{ik \cdot r}, \quad r > r_0 \quad (6)$$

where  $r_n$  is the size of the nuclear potential well. The first term represents the incident wave (wave vector  $\underline{k}$ ) and the second term the scattered wave. The scattering length  $a$  is defined as follows:

$$a = -f(0) \quad (7)$$

For  $kr \ll 1$ ,  $\psi \sim 1 - a/r$ , and we again see that  $a$  represents the distance from the origin to the point where the wave function goes to zero.

Because of the strength of the attractive nuclear potential one cannot use the Born approximation to calculate  $f(\theta)$ . However Fermi in 1936 introduced the use of a pseudo potential designed to give the result (7) when used in the Born Approximation:

$$f_{\text{Born}}(\theta) = -(mc^2/2\pi\hbar^2) * \int V(r) e^{i(\underline{k} - \underline{k}_1) \cdot \underline{r}} d^3r \quad (8)$$

It is seen that  $V(r) = (2\pi\hbar^2/mc^2) a \delta^3(r)$  gives the result  $a = -f(\theta)$ . This allows the use of the Born approximation to calculate the scattering of neutrons from complex assemblies of nuclei. It must be emphasized that  $V(r)$  is not the true potential and can only be used in the first order Born approximation.

As no accurate enough theory of nuclear structure exists, it is usual to use experimentally measured values for the scattering length. In 1950 Fermi pointed out that due to the great strength of the attractive nuclear potential, the neutron wave function will make many oscillations inside the nucleus, with the result that positive scattering lengths are much more probable than negative ones; this is actually observed.

A neutron penetrating a material medium from outside is described by the following Schrodinger Equation:

$$-\nabla^2\psi + \sum_i 4\pi a_i \delta^3(\mathbf{r}-\mathbf{r}_i) \psi = k^2\psi \quad (9)$$

where  $E = \hbar^2 k^2 / 2m = \hbar^2 k^2 / 2m$  inside the medium. Writing equation (9) as an integral equation, one obtains:

$$\psi(\mathbf{r}) = \phi(\mathbf{r}) - \frac{1}{4\pi} \int \frac{e^{ik|\mathbf{r}-\mathbf{r}'|}}{|\mathbf{r}-\mathbf{r}'|} V(\mathbf{r}') \psi(\mathbf{r}') d\mathbf{r}'^3 \quad (10)$$

from which:

$$\psi(\mathbf{r}) = \phi(\mathbf{r}) - (2\pi\hbar^2/m) \sum_i a_i \frac{e^{ik|\mathbf{r}-\mathbf{r}_i|}}{4\pi|\mathbf{r}-\mathbf{r}_i|} \psi(\mathbf{r}_i) \quad (11)$$

where the integration over the variables was performed and  $\phi(\mathbf{r})$  is a solution of the homogeneous Schrodinger equation and represents the incident wave. Equation (9) shows that  $\psi(\mathbf{r})$  is the sum of the incident wave and the waves scattered by all the nuclei and could serve as the starting point for discussing the interactions of very low energy neutrons with matter. If the neutron wavelength  $\lambda \gg d \gg a$  where  $d$  is the distance between nuclei in the material and  $a$  is the scattering length, and if the immediate neighbourhood of the nucleus be neglected, then the sum (11) can be replaced by an integral over the volume distribution of the scatterers:

$$\psi(\mathbf{r}) = \phi(\mathbf{r}) - (\hbar^2/2m) \int [N_a] \frac{e^{ik|\mathbf{r}-\mathbf{r}'|}}{|\mathbf{r}-\mathbf{r}'|} \psi(\mathbf{r}') d\mathbf{r}'^3 \quad (12)$$

where  $[N_a]_r'$  is the value of the product density in the material and the scattering length averaged over the neighbourhood of the point  $r'$ . By operating on equation (12) with  $\nabla^2$  one obtains:

$$-\hbar^2/2m \nabla^2 \psi(r) + (2\pi\hbar^2/m) [N_a]_r' \psi(r) = (k^2\hbar^2/2m) \psi(r) \quad (13)$$

which is the Schrodinger equation in the presence of an effective potential:

$$V(r) = (2\pi\hbar^2/m) [N_a]_r' \quad (14)$$

These equations have been applied to the case of reflection of cold neutrons by Steyerl (1972) and Ignatovich (1972). The solution of these equations (Goldberger and Seitz) shows that inside the medium  $\psi$  has the form  $e^{ik \cdot r}$  multiplied by a function which differs from a constant by a small amount. Here  $k$  satisfies the conservation of energy equation:

$$E' + V = E, \quad E' = \hbar^2 k^2 / 2m, \quad V = (2\pi\hbar^2/m) \sum a_i N_i \quad (15)$$

In this relation  $E'$  is the energy of the neutron in the medium and  $V$  the potential for the neutron inside the medium. Also  $N_i(r)$  is the number density of nuclear species  $i$  at position  $r$ . Values of  $V$  for various materials are presented in table 1.

Neutrons can also be absorbed by nuclei. The process can be described by a cross section  $\sigma_a$ . The cross section is related to the probability that a nucleus will absorb a neutron. If  $N_0$  be the number of neutrons incident per unit time per unit area per second on a material and  $N$  the number of neutrons which penetrate a distance  $x$  into the material, then the following relation holds approximately :

$$(N - N_0)/N_0 = -x n \sigma \quad (16)$$

provided  $\lambda \ll (n\sigma)^{-1}$ . Here  $n$  is the number of nuclei per cubic centimeter of the material. For thermal and low velocity neutrons the relation:

$$\sigma_a \propto v^{-1} \quad (17)$$

can be shown to be valid (Blatt and Weiskopf 1952). This equation expresses the fact that for thermal and subthermal neutrons the cross section of a material varies inversely as the neutron velocity. This relation is often used and holds in the case when the interaction responsible for the absorption is confined to a region much smaller than the neutron wavelength and decreases outside this region. The absorption effect can be simulated by including an imaginary component in the potential. A purely imaginary potential would cause the probability density to decay as:

$$\rho \sim e^{-2Wt} \quad (18)$$

Setting:

$$W = (\hbar/2) \sum_i N_i \sigma_a^{(i)} v \quad (19)$$

will give a correct description of the absorption as was shown by Goldberger and Seitz (1947). When relation (17) holds, then it is seen that  $W$  is independent of velocity.

## Types of Slow Neutron Scattering

### Coherent and Incoherent Scattering

The optical interference properties of neutrons are determined by the elastic coherent cross section of the individual atoms, that is, the cross section for the type of scattering that produces a wave capable of interfering with the incident neutron wave.

Coherent scattering is related to constancy of phase relations of the waves scattered by different centers. Irregular or random phase relations give rise to incoherent scattering. An important property of these types of scattering is that the amplitudes of coherently scattered waves add directly while intensities or amplitudes squared, add for incoherent scattering.

The coherence and incoherence of neutron scattering is much more complicated than the scattering of light because incoherent neutron scattering is generally larger in magnitude and arises from a number of causes that do not exist for the scattering of light. Neutron refraction resembles best the refraction of light in a gas, and as for that case, the average coherent amplitude determines the index of refraction, whereas the variation in amplitude contributes to incoherent scattering.

### Incoherent Scattering

Incoherent scattering occurs whenever deviations exist in the scattering lengths of atoms in crystals. In a crystal containing a single chemical species, variations in the scattering length from site to site will arise from the random distribution of nuclear spin orientation if the nuclei concerned have spin or from the presence of isotopes. Both of these effects are included in the cross sections for



elements quoted in the Barn Book. The incoherent elastic scattering cross section is expected to be independent of the neutron velocity and should be negligible compared to the nuclear absorption cross section and the thermal inelastic scattering cross section at the neutron velocities used in this experiment. Note that the total cross sections quoted in the Barn book include contributions from all the various types of scattering. However, in this paper, only the cross section which behaves according to the  $1/v$  law is examined. Indeed, it is the validity of this law as the neutron velocity becomes very small that is of interest.

### Inelastic Scattering

Neutron thermal inelastic scattering at very low energies occurs whenever the energy of the emitted neutrons exceeds that of the incident neutrons. Thus, the inelastically scattered neutrons gain energy and move outside the UCN or VCN range. In contrast, elastic scattering involves a change of momentum between the neutron and the whole solid which involves a very large number of atoms. Therefore the neutron neither gains nor loses energy.

The inelastic scattering described in this section differs from that which occurs at much higher energies i.e. above 100 Kev, where the emitted and incoming particles are different. This higher energy inelastic scattering is due to the nuclear excitation of the scattering nucleus and results in a scattered neutron of lower energy than that of the incident neutron.

At very low energies, the  $1/v$  law holds for the cross section for inelastic scattering, provided that the energy width of the emitted particle does not change with the incident neutron velocity.

In the case of inelastic scattering of very cold and ultra cold neutrons, where neutrons gain energy from the lattice vibrations of the scattering material, the scattered neutrons have an energy width almost independent of the incident neutron energy. Thus cold neutrons have an inelastic cross section proportional to  $1/v$ . Although the absorption and inelastic cross sections behave as  $1/v$ , they may be distinguished by the fact that the inelastic cross section refers to energy exchanges between the neutrons and the lattice vibrations (Debye Spectrum) of the scatterers. This spectrum is strongly dependant on temperature, whereas the absorption cross section, which refers to a purely nuclear

interaction, exhibits no such dependence. Since the lattice vibrations involve energies well above the cutoff energy for UCN, the neutrons which are thermally inelastically scattered are effectively lost from the UCN range.  $W$  is now determined by replacing the absorption cross section  $\sigma_a$  by:

$$\sigma_{\text{LOSS}}^{(i)} = \sigma_a^{(i)} + \sigma_{\text{INELASTIC}}^{(i)} \quad (20)$$

Henceforth the process of absorption and inelastic scattering which are both inversely proportional to the incident neutron velocity will be referred to as loss.

The magnitude of the inelastic cross section has been estimated by Binder for neutron velocities much below the characteristic excitation energy  $k\theta$  where  $\theta$  is the Debye temperature. He gives:

$$\sigma_{\text{PH}} = (S+s) (m/M) \cdot (k\theta/E)^{1/2} \cdot \left\{ 1.2 \frac{T}{\theta} - \frac{3}{7} + \frac{\theta}{8T} - \frac{1}{1560} \left( \frac{\theta}{T} \right)^3 + \dots \right\} \quad (21)$$

where  $(S+s)$  is the sum of the coherent and incoherent scattering cross sections for the bound atom,  $m$  and  $M$  are the masses of the neutron and the atom and  $T$  is the temperature. The Debye temperature for titanium is  $380^\circ \text{K}$  and at room temperature the series converges rapidly. This then gives for titanium:

$$\sigma_{\text{INEL}} \sim 130 v^{-1} \quad (22)$$

This will be compared to the measured loss cross section in the discussion of the results which follow later.

### Inhomogeneous Elastic Scattering

In polycrystalline and non uniform substances, additional effects arise due to fluctuations in density brought about by a disorder in structure. In alloys this effect will be further complicated by fluctuations in the composition on a microscopic scale. The elastic scattering cross section from such inhomogeneities varies inversely as the incident neutron energy over a fairly wide range of energies, but tends to be energy independent at very low energies (typically whenever the wavelength of the incident neutron exceeds by three times the order of the inhomogeneity spacing). At higher energies where the scattering angles are small, it varies more rapidly, inversely as the square of the incident energy of the neutron. This type of inhomogeneity scattering has been investigated in some detail by small angle scattering of cold neutrons (Schmatz et al 1974) and more recently by total elastic scattering cross section measurements of VCN (Steyerl and Englemann 1979). In this experiment the effect of inhomogeneity scattering will be small for two reasons. First, the titanium foil was quite pure (see page 72) and thus would not have inhomogeneities in composition though it may have had irregularities in its microcrystal structure; secondly the foils used in the experiment were mounted directly in front of the detector so that most neutrons scattered by this process would still have been detected and would not have contributed to the measured loss of intensity. The titanium foil used in this experiment was analyzed by the chemistry division at ACEL. This analysis indicated that the contributions of the impurities to the thermal cross section was considerably less than one percent of the thermal cross section. In the interpretation of this experiment it is therefore assumed that

inhomogeneous elastic scattering had a negligible effect. The fact that the loss cross section agrees well with a  $1/v$  extrapolation from measured thermal cross sections gives some confirmation to this assumption.

#### Bragg Scattering

Diffraction by a set of lattice planes can take place if the neutron wavelength is smaller than the lattice spacings in the crystal. Ultra cold neutrons have energies of order  $10^{-7}$  electron volts. The wavelength associated with a neutron in this energy range is a few hundred angstroms, whereas the lattice spacing in a crystal is only a few angstroms. Therefore Bragg Scattering plays essentially no role in UCN and VCN scattering. In titanium the lower cut off energy is expected to be .004 volts (lattice spacing for a crystal is 4.68 angstroms). However in comparing the cross sections measured in this experiment with those to be expected from an extrapolation of the literature values in the region .002 ev. to 50 ev., Bragg scattering occurring in the latter energy range can cause difficulties in interpreting the experimental results. This point is discussed further on page 34.

### Total Reflection of Neutrons from Material Walls

We can consider the surface of a material with a positive scattering length as constituting a potential barrier. If a neutron has a kinetic energy in the direction of the normal to the surface, satisfying the relations:

$$E_{\perp} < V = (2\pi\hbar^2/m) \sum_i N_i a_i \quad (23)$$

it cannot penetrate the surface according to the laws of classical mechanics, hence is totally reflected. Quantum mechanics allows for surface penetration, with the probability of transmission given by relation (18). For neutrons of velocity  $v$  travelling at an angle  $\theta$  with respect to the surface the perpendicular kinetic energy  $E$  and the critical angle are given by the relations:

$$E_{\perp} = \frac{1}{2} m (v \sin \theta)^2; \quad \sin \theta_c \leq (V/E)^{1/2} \quad (24)$$

This condition is equivalent to saying that the perpendicular kinetic energy  $E$  should not exceed the scattering potential for total reflection.

To treat the reflection quantum mechanically one can assume a surface whose roughness is on a scale much smaller than a neutron wavelength. In this limit the surface may be treated as an abrupt potential step. A surface extending over a region much larger than a wavelength is equivalent to a one dimensional potential. The probability of reflection from a potential barrier of height  $U$  is obtained by applying the boundary conditions to the solution of the Schrodinger Equation. The potential  $V$  is the real part of the complex potential  $U = V - iW$ . If  $U$  does not allow for absorption then  $V$  must equal zero. Using a real potential,

the probability of reflection is:

$$|R|^2 = [(E_1)^4 - (E_1 - U)^4] / [(E_1)^4 + (E_1 + U)^4] \quad (25)$$

If  $W$  is real and  $E \ll U$  then  $|R|^2 = 1$ . For a complex potential and to first order in  $W$  with  $E \ll U$  one finds:

$$|R|^2 = 1 - 2f(E_1/V - E_1)^{1/2} = 1 - \mu(E, \theta) \quad (26)$$

where:

$$f = W/V = 1/2 (\sigma_L / \lambda_0 a) \ll 1 \quad (27)$$

An exact expression for  $|R|^2$  is given in Luschikov et al (1968) and Antonov et al (1969). Table 1 shows values of  $f$  for some interesting substances. As previously noted  $W$  and  $V$  and therefore  $f$  are independent of neutron energy. This means that  $f \ll 1$  even at the energies of UCN energy where loss cross sections are often much larger than the coherent elastic scattering cross section  $4\pi a^2$  and the presence of loss will not significantly change the wave function. Since its first observation by Fermi and Zinn in 1946 total reflection of neutrons has been widely used for the determination of scattering lengths as well as for polarizing neutrons in guide tubes where neutron beams are confined in two dimensions.

### Production of UCN

Neutrons are generally produced as the result of a nuclear reaction or fission process. In either case neutrons are produced with kinetic energy of several Mev or higher. In order to obtain neutrons with thermal or lower energies it is usual to surround the source with some material which scatters the neutrons, gradually absorbing the neutron energy by recoil of the scattering nuclei. If this moderator consisted of materials whose nuclei did not absorb neutrons and was of infinite size, the neutrons would eventually come into thermal equilibrium with the moderator and the energy spectrum would be Maxwellian corresponding to the temperature of the moderator. In any real system both absorption and boundaries are present and so the thermalization is not complete. The neutron energy spectrum may be approximated by a Maxwellian distribution corresponding to a temperature slightly higher than the temperature of the moderator. An increase in the flux of the neutrons at energies below that corresponding to room temperature is possible by cooling the moderator. The neutron spectrum may be described by the Maxwell distribution given by (1).

The density of UCN neutrons available for trapping in a cavity whose walls have a potential  $V$  is given by:

$$\rho_{ucn} = \int_0^{v_c} n(v) dv = \int_0^{v_c} 4\pi n_0 (m/2\pi kT) e^{-\frac{1}{2}mv^2/kT} dv \quad (28)$$

This equation represents the maximum UCN gas density that can be obtained from a given source at a given temperature if the UCN are in thermal equilibrium with the moderator.

There are effects which occur in the moderator which reduce the available UCN density below that given by the above calculation. Since



UCN are produced by neutrons colliding with moderator nuclei, and losing most of their energy upon the first impact, it is not unreasonable to assume that a lack of low frequency vibrational modes of moderator nuclei would cause anomalies in the tail end of the Maxwell distribution.

If it is required to extract some UCN from the moderator and trap them in a closed container, then one is faced with the problem that the only neutrons which can enter the cavity by penetrating the walls will have too large an energy to be contained by the walls. There are several ways of surmounting this difficulty however. One can fit the moderator with a window made of a material whose potential energy is considerably lower than that of the material forming the walls of the container or place some material which is capable of converting neutrons from  $E > V$  to  $E < V$  inside the container. In order to calculate the UCN density available for a moderator which may be either the converting material (called the converter), or the moderator adjacent to the window, one should note that the total loss cross section for UCN, which is the sum of capture and inelastic scattering cross sections can be very large since both these cross sections vary as  $1/v$ . Hydrogenous substances have a total mean free path of about  $3\mu\text{m}$  for 25 mv neutrons. The only UCN which are able to emerge from the material are those which reach the UCN energy range within a distance of the order of  $\lambda_{\text{UCN}}$  from the surface, hence it is only necessary to consider this thin surface layer in calculating the production of UCN. However, the energy distribution of the neutrons incident on this active layer may be modified by the remainder of the moderator material. The number of UCN produced in an energy range between  $E$  and  $E+dE$  per unit volume of moderator per second may be second

may be written as:

$$S(E_{UCN}) dE_{UCN} = \int_0^{\infty} dE \sum_s (E \rightarrow E_{UCN}) \Phi(E) dE_{UCN} \quad (29)$$

The macroscopic differential energy cross section is:

$$\sum_s (E \rightarrow E_{UCN}) = N \frac{d\sigma_s(E \rightarrow E_{UCN})}{dE_{UCN}} \quad (30)$$

where  $N$  is the density of atoms in the moderator material and  $d\sigma_s(E \rightarrow E_{UCN})$  is the macroscopic differential cross section for scattering neutrons of energy  $E$  into the energy range  $E_{UCN}$ . Here  $\Phi(E)$  is assumed to be homogeneous and isotropic. The UCN produced travel through the moderator until they are captured or scattered inelastically (in which case they leave the UCN energy range) or are elastically scattered. In the absence of elastic scattering one obtains the flux of UCN leaving the surface of the moderator by multiplying (27) by the effective thickness of the active layer described above :

$$\gamma = (\sum_{\text{INELAST}} + \sum_{\text{CAPTURE}})^{-1} \quad (31)$$

A calculation by Golub (Golub 1972) shows that the emitted flux is given by :

$$J(E_{UCN}) dE_{UCN} = \frac{1}{4} \{ S(E_{UCN}) dE_{UCN} \} \gamma_{UCN} \quad (32)$$

where:

$$\sum_{\text{INELAST}} (E_{UCN}) = \int_0^{\infty} \sum_s (E_{UCN} \rightarrow E) dE \quad (33)$$

For materials in thermal equilibrium, one can write:

$$\sum_s (E \rightarrow E_{UCN}) E e^{-E/kT} = \sum_s (E_{UCN} \rightarrow E) E_{UCN} e^{-E_{UCN}/kT} \quad (34)$$

where  $T$  is the temperature of the material. Using this result and assuming that the incident neutron flux is given by a Maxwellian spectrum corresponding to temperature  $T$  and total flux  $\phi_0$ , one has:

$$\phi(E)dE = \phi_0 E e^{-E/kT} / (kT)^2 = \phi_0 f_T(E) \quad (35)$$

which is determined by conditions external to the active layer and which can be calculated by standard methods, (Davison and Sykes, 1957, Egelstaff and Poole, 1969). Equation (27) may be written as

$$\int (E_{uN}) dE_{uN} = \phi_0 f_T(E) \left( \frac{T}{T_0} \right)^2 \int \sum_s (E \rightarrow E) e^{-\frac{(T_0 - T)}{T_0 T}} \quad (36)$$

Thus it is seen that the flux emerging from the moderator is a Maxwellian distribution times a correction factor. This factor is practically independent of  $E_{uN}$  so that the UCN spectrum will be the low velocity end of a Maxwellian spectrum.

## Chapter Two

### Experimental Procedure

This experiment may be divided into two dependent parts. In the first part, a horizontal beam of UCN was subjected to various constraints which allowed measurement of the number of neutrons emerging in a given solid angle. From this preliminary work it was also possible to estimate the specularity of the guide tube, a consideration necessary to the interpretation of the central second experiment. In the second part the attenuation of various titanium foils was measured.

The source of neutrons was the NRU reactor at Chalk River. In order to extract the UCN from within the thermal column, the arrangement illustrated in diagram 1 was used. The converter consists of a thin polythene disk attached to a copper tube. This converter was cooled to liquid nitrogen temperature to enhance the production of UCN by a factor of approximately two. The copper tube was evacuated to a pressure of tens of microns of mercury to minimize the interaction of neutrons with air.

To separate the more energetic neutrons from UCN, the geometry illustrated in diagram 2 was utilized. This arrangement makes use of the properties of UCN described in the introduction. The horizontal guide tubes beyond the bends were made from mechanically polished stainless steel. To prevent thermal neutrons from entering the guide tubes, a sheet of 1/16 cadmium was wrapped around their outer surfaces. The transmission of higher energy neutrons was minimized by placing borinated paraffin blocks in appropriate positions. Paraffin converts high energy neutrons to thermal neutrons so that they can be captured by the boron. It should be noted that diagrams one and two are not drawn

to scale.

The neutron guide tube was connected to the velocity spectrometer or chopper. The chopper is a rotating disk containing one circular hole of the same diameter as the guide tube that transmits bursts of neutrons at regular intervals. These neutrons travel to the detector over a measured path. Electronic circuits time the interval between the opening of the chopper and the response of the detector. These circuits and the detector will be described below.

The chopper used is shown in diagram 3. The shutter is an off centered hole bored in two aluminum disks. The space between the disks is filled with cadmium foil to absorb any slow neutrons while the shutter is closed. This assembly is supported by a shaft which goes through the center of the disks and is enclosed by a hermetic housing permitting free rotation of the shutter. The chopper was driven by a DC shunt type motor whose rotational speed could be controlled by varying its input voltage. The difficulty with this kind of motor is its tendency to drift, necessitating careful monitoring of the rotational speed.

The circuitry may be divided into a timing and a detection section. To obtain a timing signal, a circular hub was attached externally to the chopper shaft. This hub had one small hole bored through it as shown in diagram 3. The hub had to be aligned, so that a pulse could be generated only when the shutter was fully open. This pulse indicated the arrival of neutrons and acted as an external trigger for the multichannel scaler (MCS). Before the photodiode pulse could be used as a timing signal, it required shaping and amplification. To accomplish this, a DC preamplifier was designed and built to accept the 0.15 volt diode pulse

and to generate a digital pulse having the same time- amplitude characteristics as the original signal. This pulse was then amplified further to 1.5 volts and fed into a discriminator. The discriminator upon receiving this pulse produced a very fast delta function type blip which triggered the MCS. The block diagram of this circuitry is illustrated in diagram 4. This timing signal was also fed into a scaler which could be made to count for one minute, delay for a specified time clear and recycle. In this way a constant monitor of the rotation speed could be maintained. The rotational speed of the chopper was  $240 \pm 3$  rpm.

The detection system consisted of a boron trifluoride detector and associated amplification and discrimination circuitry. The detector was filled with 1.6 cm of  $\text{BF}_3$  and 37cm of helium. The relatively low  $\text{BF}_3$  pressure decreased the detector sensitivity to higher energy neutrons but retained a high sensitivity for UCN and VCN. The detector window consisted of a .001 inch thick titanium foil supported by a stainless steel grid.

Detection is based on the  $(n,\alpha)$  reaction in boron 10 which has the large thermal cross section of 4010 barns. The particles released, alpha particles and lithium 7\* nuclei, produce high specific ionization in gases. Therefore, these particles are readily detected in the presence of other, weaker ionizing particles such as secondary electrons from gamma rays. By use of circuits which discriminate against pulse heights below some selected level, the gamma ray background can be suppressed.

Since the output pulses from the detector were too small to be usable, preamplification was necessary. After preamplification, the signal was further amplified and fed into a discriminator. To properly set the lower window of the discriminator so that the signal to noise ratio

could be maximized, it was necessary to obtain the characteristic response curve of the detector. To do this, a strong neutron source (Am-Be) embedded in paraffin wax was placed in close proximity to the detector and the amplified signal arising from the detector was fed to the input of the ADC of the MCA. The spectrum illustrated in fig 3 was obtained. The first peak in this curve corresponds to gamma ray activity and electronic noise. The second rather large hump corresponds to the neutron detection signal. Thus the discriminator was adjusted to reject the noise and allow passage of signals just below the second hump (shaded area 1-2).

It should be noted that the broadness of the second hump was due to the geometry of the detector which was three inches in diameter but only one inch deep; this was chosen to optimize the UCN/thermal detection efficiency but is not ideal as a proportional counter. To calibrate this spectrum a pulser was used. By varying the output voltage, the pulse could be made to move either to the left or to the right as seen on the MCA. The voltage was thus set so that the pulse arrived at the desired location. This voltage setting was chosen for the lower window of the discriminator.

To minimize the detection of background thermal neutrons originating elsewhere in the reactor hall, it was necessary to envelope the detector in a cadmium shroud. Suppression of more energetic neutrons was accomplished by constructing a borinated paraffin enclosure around this cadmium.

To measure the flux as a function of solid angle subtended by the detector, various lengths of polythene liner were inserted inside the guide tube. The neutron count corresponding to a given length of liner

was recorded. To verify that UCN and VCN were indeed being propagated down the guide tube, a polythene disk was inserted to seal the guide. In this manner, the presence of these neutrons was confirmed as the count rate was much diminished. Furthermore, it was found that there was no significant difference in the count rate by either increasing or decreasing the thickness of the disks over the range .08 to 1 cm. This constant rate could, in fact, be used for determining the background noise. The chopper was not used in this phase of the experiment.

To check that this constant rate was due to thermal and higher energy neutrons, the disks were removed and replaced by a single cadmium sheet 1/16". This sheet was so placed that it covered the sensitive front end of the detector. It was observed that this counting rate did not differ statistically from the counting rate obtained with the disks in place. It should be noted that cadmium cuts thermal neutrons down the tube but nothing else.

In fig 4 the results obtained with and without background correction are shown. The large background is probably the result of insufficient shielding around the detector. The results and interpretation of this experiment will be discussed in the next chapter.

In the second part of the experiment an attempt was made to determine the attenuation of various titanium foils for neutrons of various velocities using the chopper described above. In a later section of this thesis, this attenuation is interpreted as a loss cross section. Measuring this attenuation involves recording the neutron counting rate as a function of foil thickness. The interpretation of such transmission measurements is clearer if the incident neutrons are collimated in a beam rather than randomly oriented in angle. An attempt was made to



achieve this by placing a liner inside the neutron guide tube just ahead of the detector. The liner was made of polythene 10 cms long and 0.16 cms thick; it was essentially opaque to neutrons used in this experiment. Thus the neutrons which were detected were partially collimated; a discussion of this point will follow later.

The velocity of the impinging neutrons, and hence their energy could be deduced from their time of flight (TOF) spectrum. A sample spectrum is shown in fig 5. The first large peak represents all fast and thermal neutrons that passed through the chopper and were hence timed. The second peak may be divided into two parts. The positive slope represents the VCN spectrum, whereas the negative slope derives from the UCN contribution. Not far beyond the UCN portion there should in theory be no counts. One can calculate that the minimum velocity should be about 2 cm/sec. In practice, one does not see this because of the very low flux predicted by the Boltzmann Distribution of neutrons having this velocity, the poor resolving power of the chopper and the absorption of the thin titanium window on the detector. These points falling beyond channel 360 correspond to background; that is, neutrons entering the detector from all angles. Because these neutrons are not timed, they appear as points spread uniformly throughout the spectrum.

### Chapter Three

#### Interpretation of Results

In the first part of this experiment the counting rate of the neutron detector was measured as a function of various lengths of polythene liner. The liner was placed inside the guide tube just ahead of the detector. It seems reasonable to assume that the polythene of thickness 0.16 cm was opaque to all UCN and VCN since hydrogen has large inelastic and absorption cross sections.

In view of the fact that there exists a critical angle of reflection given by equation 2, the VCN will be limited to trajectories which make small angles to the surface of the tube. VCN are thus less likely to strike the liner than the UCN, many of which will make large angles to the surface. This point is illustrated in diagram 5. It might thus be expected that the variation in the number of neutrons striking the central region of the detector, as a function of liner length for both VCN and UCN, will be of the general form shown in fig 6. The difference in behaviour of the two types of neutrons can be used to give some information on the velocity spectrum of the neutrons transmitted down the tube. As will be shown, the velocity spectrum is sensitive to the degree of specularity of the reflections at the surface.

To obtain an estimate of the number of UCN transmitted down the guide use was made of a Monte Carlo computer program previously developed at McGill. The program assumes no losses of UCN around the bends, a reasonable assumption for 100% specular reflection but inappropriate for diffuse reflection. Since few reflections (probably 3 or less) are involved at each bend, and a high degree of specularity is expected, the

assumption of a large specularity is probably acceptable. In order to test the effect of the polythene liner and to include the absorption in the counter window, it was necessary to modify the program for the appropriate boundary conditions. The results are shown in fig 7 for various degrees of specularity. The agreement with the experimental results is not good. However, a comparison with fig 6 suggests that the addition of some VCN would modify the predictions in the correct direction to better correspond with the experimental data.

In order to estimate the transmission of VCN it is necessary to take a more realistic account of the bends effect. To do this, a three dimensional Monte Carlo calculation should be performed. The difficulties in developing and debugging such a complicated program led to the use of a two dimensional analogue previously developed by the McGill group as part of a general computer simulation of the passage of UCN and VCN down neutron guides. In this two dimensional code, neutrons of a given velocity were followed around two bends connected by a straight section. Repetition of this procedure for various velocities yielded the transmission factor for this filter, which after multiplication by  $v^3$  gave the predicted VCN spectrum for neutrons entering the final straight section containing the polythene liner. The factor  $v^3$  enters from the low velocity approximation to the Boltzmann Distribution.

Figure 8 shows the predicted velocity spectrum for various lengths of straight section between the bends. This result assumes 100% specularity around the bends and includes the necessary correction for the efficiency of the detector. This factor approaches unity for the UCN but drops off as the velocity exceeds the UCN limit due to the low BF<sub>3</sub>.

pressure.

It should be noted that a short connecting section between the two bends is predicted to filter out the VCN more effectively than a longer one. This effect is due to the bunching of VCN near the bottom of the first bend which would result in their striking the second bend surface at an angle exceeding  $\theta_c = \sin^{-1}(V/E)^{1/2}$  and be lost. However, a longer straight section redistributes these neutrons and enhances the transmission of the second bend.

The straight section separating the bends was 33 cms long. The 100 cm velocity spectrum is shown as a time of flight spectrum in fig 9 for the situation of the velocity spectrometer used in the experiment. Also shown is the spectrum modified by the time resolution function of the chopper.

To use this spectrum as a base for predicting the effect of VCN on the polythene liner experiment, the previously mentioned UCN Monte Carlo program was modified by the addition of VCN. This modification allowed for the possibility of loss at a wall collision due to the neutrons incident angle exceeding the cutoff value for its particular velocity. The spectrum coming out of the second bend was used as the incident spectrum for this calculation. The results are shown in fig 10. In this figure, the result for 80% specularly for pure UCN is shown and is seen to be too low, whereas if the same specularly is assumed for VCN only, it is seen to be too high. The other curves are for the mixture of UCN and VCN predicted by the bend calculation, shown for 100%, 80% and 60% specularities. The curve for 80% specularly with both UCN and VCN is in reasonable agreement; far better than the results for pure UCN.

### Interpretation of the Attenuation Experiment

The attenuation experiment provided the data necessary to deduce the UCN absorption cross section for titanium foil. Titanium has a negative scattering length. This means that it transmits a fraction of the incident UCN beam. This fraction can be related to the loss cross section since those neutrons suffering nuclear absorption are lost, and those inelastically scattered have energies too high to be detected by the  $\text{BF}_3$  detector.

The first step in the analysis is to determine the level of background noise. This noise arises from the detection of stray neutrons of varying energies arising elsewhere in the reactor hall. Since the noise level was never constant it was necessary to estimate where the base line should be, the estimate being based on the fact that neutrons having velocities less than 3 m/sec are not detected with the existing system. To draw the base line, the counts in the channels corresponding to velocities below 3 m/sec were summed and averaged, thus establishing the noise level. Justification of this procedure is founded in experimental observations of the noise levels when the thermal column was closed. With the chopper running, it was seen on the MCS that the background level was time dependent, i.e., changing from run to run. This being the case, it is not unreasonable to subtract the averaged background from the total spectrum in the manner indicated.

The analysis of the data leading to the interpretation of this experiment would be a relatively simple task if the VCN and UCN neutrons moved in straight lines instead of rebounding off the walls of the guide tube. One could in practice line the entire guide tube with polythene, ensuring linear trajectories, however, the already low flux of UCN and

VGN neutrons would diminish very considerably and result in a practically nil counting rate. The best one could do to collimate the neutron beam was to only partially line the guide tube with polythene. This was done and the results of this effort have been discussed in the previous section.

Using Monte Carlo programs, it was possible to obtain curves which approximated the observed data. More specifically, it was possible to determine the trajectories of both species of neutrons as a function of specularity and length of polythene liner down a tube of length 80 cm. The results are shown in table 2. In this table,  $l$  is the length of polythene liner,  $F$  is the assigned specularity of the guide tube and  $x$  is the average path length of a neutron. The average path length of a neutron is calculated by dividing the total distance travelled by many neutrons by the number of neutrons detected, using a given specularity. The geometrical factor  $F$  allows for the calculation of the total axial distance travelled by a neutron. This factor is equal to  $\sec(\theta)$  as shown in diagram 5. Now the total axial length a neutron must travel before reaching the detector is: 1 cm (for chopper) + 50 cm (path length) +  $\lambda_D$  where  $\lambda_D$  is the mean free path of a neutron having a velocity of 5.7 m/sec in the detector. The total path length is therefore 52.2 cms times the factor  $F$ . The path length between chopper and detector was 50 cm; the value of  $F$  calculated from the Monte Carlo calculation for a tube of length 80 cms were assumed to be valid for this 50 cm tube.

Because of the poor resolving power of the chopper, better statistics could be obtained by grouping the data in bins of twenty. The contents of the first twenty channels were summed and reassigned to the first channel. Similarly the contents of the next twenty channels were summed

and were reassigned channel two and so on thus smoothing the data.

hence, the  $n$ th channel corresponds to a time:

$$t = \{20C_{10n} - 10\} \times .4 \quad (37)$$

The factor .4 ms comes from the time base of the MCS. This means that the dwell time per channel is .4 milliseconds during its scanning mode.

The velocity is given by the expression:

$$V = 522 F / \{8C_{10n} - 4\} \quad (38)$$

For a 10 cm length of polythene liner, the values of  $F$  given in table 2 are too large for both UCN and VCN neutrons. It was necessary to interpolate using fig 16 to obtain a new value for  $F$  which results in a lower critical angle for both species of neutrons. Figure 16 was not derived experimentally but was obtained from a Monte Carlo simulation. The plot reveals the variation of the secant of the critical angle ( $F$ ) as a function of neutron velocity.

For UCN having velocities in the range from four to about six meters per second the best value for  $F$  is 1.4 while that for VCN is 1.25. Using these values a plot was made of velocity against channel number the results of which are shown in fig 11. As may be seen the linear portion of the curve extends from channels 12-22. Three points in this region were selected to deduce the cross section of the titanium foil. The points in fact correspond to areas or total counts. Table 3 shows these divisions. The total area under the sections of interest was obtained from the original data with the background subtracted. It will now be shown how the cross section of titanium at different neutron velocities may be inferred from the data. By plotting the integrated

counts against the thickness of titanium foil, one obtains curves such as those shown in fig 12. The slope gives an apparent mean free path denoted by  $q'$ . Here use is being made of the relation :

$$N = N_0 e^{-x/q'} \quad (39)$$

In fact, it is necessary to plot counts versus true path  $r$  in titanium foil, not  $t$ , its thickness. From the relations:

$$x = Ft, \quad q = Fq' \quad (40)$$

one obtains the actual mean free path  $q$ .

The calculation of the cross section requires the velocity of the neutrons inside the foil. Using Snell's law, one obtains the relation:

$$v_i = v \left\{ 1 - (v_c/v)^2 \right\}^{1/2} \quad (41)$$

In this equation  $v$  is the neutron velocity inside the foil and  $v_c$  is the critical velocity for titanium which is 3.08 meters per second. The expression 3.08 $i$  where  $i = \sqrt{-1}$ , indicates that the scattering length is negative. Table 4 shows the resulting cross sections of titanium for the mean velocities of the three bins used in the data analysis. To obtain the loss cross section  $\sigma_{\text{loss}}$ , literature data for titanium was plotted assuming a fitting function of the form:

$$\sigma = \alpha v_0/v + D, \quad \sigma_{\text{loss}} = \sigma - D \quad (42)$$

The least square fitting procedure applied to the literature data gave  $\alpha = 6.6$  barns, and  $D = 4.07$  barns. Here  $\sigma$  is the observed cross section,  $\alpha$  the normalized cross section for 2200 meter/sec neutrons,  $v_0$  the most probable velocity of the Maxwellian distribution ( $v_0 = 2200$  meters/sec at



$T=20^{\circ}\text{C}$ ) and,  $v$  the incident neutron velocity. The constant  $D$  represents that part of the observed cross section which does not follow the  $1/v$  law. It includes contributions resulting from Bragg scattering, incoherent scattering and all other types of scattering for neutrons in the range of  $10^3$  to  $10^4$  meters/sec.

The observed points in this experiment were then placed on the fitted curve, which had been extrapolated to the velocity range of interest. It should be noted that the constant  $D$  is small, being only about 4.07 barns. However, there does exist some ambiguity in the meaning of  $D$  at very low energies. For example there cannot be Bragg scattering for energies in the range  $10^{-6}$  to  $10^{-7}$  electron volts since the neutron wavelength is a few hundred angstroms. Yet for thermal neutrons, Bragg scattering is not uncommon.

As mentioned on page 14 the effect of Bragg scattering complicates the fitting function for the literature data since it is essentially zero below .004 ev. In fact, a non critical glance at the data for the total cross section might suggest the presence of an edge in the region near 0.004 ev. To test this, a fit of the literature data was performed over two regions: from .002 to 50 ev. and from .004 to 50 ev. The former region yields  $D=4.07$  barns while the latter results in  $D=3.98$  barns. The difference in the loss cross sections was .15 barns. This suggests that the effect of any Bragg scattering does not seriously affect the interpretation of this experiment.

### Sources of Error

In this section the sources of error will be discussed and ideas will be presented to improve the experiment.

There are three sources of error that affect the data. These errors arise from: the low resolving power of the chopper, a time varying neutron flux, and system timing errors, all to be described below. Of these, the first two contribute relatively large errors.

The resolving power of the chopper is inherently dependant on its design and construction. A larger chopper having a slit instead of a circular shutter would increase its sensitivity to velocity discrimination but would reduce its transmission. For example, instead of grouping the data in lots of twenty as was done in the analysis of this experiment, it would be better to group the data in smaller lots, allowing more points to be used thus increasing the accuracy in the cross section versus velocity graph. The resolving power of the chopper is given by the expressions:

$$\Delta t = (r/\pi R) * f^{-1} ; f = 4 \text{ sec}^{-1} \quad (43)$$

Inserting the appropriate numbers it is found that the time resolution of the instrument is 48 msec for a rotation speed of 240 revolutions per minute. For a 6 meter per second neutron this means a velocity spread of  $\pm 1.7$  meters/sec. Since the resolution also depends on the length of the flight path, an increase in its length would improve the resolution.

As always however there is an exchange. This exchange would result in a decrease in the counting rate which would adversely affect the statistics. Some mechanisms which conspire to yield a low counting rate will be described later.

An inspection of column five in table 4 reveals that the normalized cross section for 2200 meter/second neutrons is not constant. This result is partly due to the low resolving power of the chopper. The velocity resolution of the chopper is given by the expression:

$$dv/v = .096 v \quad (44)$$

To calculate the error in the normalized cross-section  $\sigma_0$ , one uses the result :

$$d\sigma_0 = (v d\sigma + \sigma dv) / v_0 \quad (45)$$

to obtain:

$$d\sigma_0 \approx \left(\frac{1}{4}\right) * \sigma \frac{dv}{v_0} \quad (46)$$

This assumes that the velocity resolution of the chopper remains constant. In fact, the velocity resolution is given by equation multiplied by  $\epsilon_d$ , the efficiency of the detector. It turns out however that the efficiency of the detector does not vary wildly for neutrons in the range 6.8-8.0 meters/sec. For a 6.8 meter/sec neutron, the error in  $\sigma_0$  is  $\pm 2.3$  barns.

The error in the loss cross section  $\sigma_{loss}$  must be found by first determining the error in the apparent mean free path and then using the result:

$$\frac{d\sigma_{loss}}{\sigma_{loss}} = \frac{dF}{F} + \frac{dq}{q} \quad (47)$$

The error in the apparant mean free path was determined by applying a least squares fit to the counts versus titanium foil data. To determine

the error in  $F$ , a plot was made of  $F$  as a function of velocity. Values of  $F$  as a function of velocity were obtained from the Monte Carlo program described previously by holding the specularity fixed at 80% and keeping the length of the polythene liner fixed at 10 cms. Thus, the only variable input was the initial velocity of the neutron. From the curve obtained in this manner (see fig 16) it was possible to estimate the error in  $F$ . The way the error was computed is best shown by an example: if it is required to find the error in  $F$  for neutrons having velocities in the range from say 6.5 to 7.4 meters per second (corresponding to area one in fig 17) one obtains from fig 16 values of  $F$  corresponding to 1.36 and 1.26. The difference divided by two is the error associated with a neutron having an average velocity of 6.95 meters per second, or the mean of 6.5 and 7.4 meters per second. It should be noted that there exists another source of error in  $F$ . This error is associated with the way  $F$  was obtained in the first place- a Monte Carlo simulation. This error is straightforward to compute and is given by the expression:

$$e_f = \sum_i (\bar{F}_{av} - F_i)^2 / N_D ; N_D = \text{neutrons detected. (48)}$$

This error is small however and therefore not included in the error in  $F$ .

One major drawback to working with an engineering type reactor lies in the frequent changes in flux level. Because fuel bundles are periodically changed or moved to another position in the reactor lattice in order to maintain constant power, the flux in a given location may vary by as much as ten or fifteen percent. In order to obtain consistent results, it was necessary to monitor the neutron counting

rate near the guide tube. An external counter was placed in close proximity to the guide so as to normalize the counting rate, i.e. make it independent of reactor power. Unfortunately, the counting rate did not depend on the power in a linear way for reasons which were not explored due to lack of time. To surmount this problem the flux in the experimental area was monitored by detectors placed inside the reactor. These counters could monitor the flux accurately to within 5%. Measurements were thus taken only when the neutron density was constant as indicated by the counters. Thus, an error of 5% can be associated with the UCN counting rate due to flux variations. As a first approximation it was assumed that the percentage of UCN is always the same i.e., the ratio of UCN to the total neutron population at all energies is fixed so that if the flux of neutrons varies by 5% the UCN flux will vary by 5%.

## Loss Mechanisms for UCN and VCN

### Pores and Surface Roughness

The probability of losing UCN in the walls of the guide tube is increased if the pores in the material, which constitute the guide tube, are of order 100 angstroms or greater. If the size of the pores is much smaller than the UCN wavelength the average density of material and hence the UCN potential  $V$  will be reduced. If in addition the porosity is a function of distance from the surface the effective potential might have the form shown in fig 15 instead of the ideal form shown in fig 14. This could increase the UCN losses because the UCN penetrate further into the material; however this can only have a minor effect. If on the other hand the pores are of the order of a UCN wavelength, then UCN can be trapped in a pore with a consequent increase in loss rate.

In the opposite extreme if the wavelength of the UCN is much larger than the size of the pores in the guide, the effect will be to round off the potential step of the ideal surface as in fig 15 and this will increase the UCN loss rate since the UCN wave will overlap a greater number of nuclei before reflection. This problem has been studied in detail by Ignatovich (1973) who treated the problem by applying perturbation theory to the Schrodinger equation assuming a Gaussian correlation function for the surface roughness with the result:

$$\bar{\mu} = \mu_0 * \left\{ 1 + 2b^2 k_c^2 / (1 + 6k_c w + (k_c w)^2)^{1/2} \right\}^{1/2} \quad (49)$$

where  $\mu_0$  is the loss factor in the absence of pores and  $k_c = \left( \frac{2mV}{\hbar^2} \right)^{1/2}$  is the critical wave number for UCN reflection, and  $b$  the rms height variation of the surface roughness. For typical parameters  $b \sim 50 \text{ \AA}$ , and  $k_c \sim 10^8 \text{ m}^{-1}$ , taking

the worst case  $W \rightarrow 0$  one finds an increase in UCN losses of about 25%.

#### Losses due to impurities

One mechanism which may be responsible for some UCN loss is related to impurities on the inner surface of the guide tube. In order for large losses to occur it would be necessary that the contaminant have a small nuclear mass and a large incoherent cross section (Blokhintsev and Plakida, 1977). A prime candidate having these properties is hydrogen. In addition it should be noted that because of its chemical properties hydrogen could be present to some extent, in the form of hydroxides in the oxide layer which covers most metals. Hydrogen can also be deposited on the inner surface in the form of a hydrocarbon by the vacuum pump which uses oil, although the geometry used minimizes this effect. Nevertheless it has been estimated that a hydrogenous layer about  $70 \text{ \AA}$  thick would cause large UCN losses (Herdin, et al, 1977). From the foregoing discussion it is evident that a highly polished guide tube void of surface contamination would minimize UCN losses, thus allowing for a longer flight path. The guide tubes used in this experiment were only mechanically polished; the use of electroplating or ion bombardment might have reduced the UCN losses by reducing the very sharp surface imperfections and by more effectively cleaning the surface layer.

#### Losses Resulting from System Timing Errors

The system timing errors are of two kinds: those resulting from timing errors of the MCS during its sweep cycle and those attributed to fluctuations in the rotation speed of the chopper. The former could

result in gross errors if the sweep control was not properly calibrated. However, this system was checked and was deemed reliable. Since the rotation speed of the chopper was manually controlled by varying the input voltage to the motor, it is clear that a constant speed cannot be maintained over extended periods. This fluctuation in rotational velocity results in asynchrony with the MCS time sweep and causes the MCS to miss timing some of the UCN bursts. The effect is to diminish the neutron counts. To regulate the rotation speed it is recommended that a feedback system be employed with a DC motor or a synchronous motor. Such a system would also free the operator from maintaining a constant watch over the motor.



### Conclusion

The object of this experiment was to determine the attenuation of UCN by titanium foil. This attenuation could, after appropriate transformation, be interpreted as a loss cross section. It was found that the loss cross section was consistent with the  $1/v$  law, although it appears that the cross section deviates increasingly from this law as the neutron velocity becomes nil. The errors are large, and points few to say that aberrations from the  $1/v$  law exist at extremely low velocities. A more accurate experiment would have to be performed in order to verify this observation. The loss cross section defined on page 12 results from inelastic and absorption effects. It should be noted that the inelastic scattering cross section also varies as the  $1/v$  law.

The thermal inelastic cross section at 6.95 m/sec is estimated to be nearly 20 barns from the expression given on page 12. This is small in comparison to the measured loss cross section of 1800 barns suggesting that most of this loss is due to nuclear absorption in the case of titanium.

Titanium was selected because it is characterized by a negative scattering length, which means that it permits some transmission of UCN and VCN. Its ability to transmit extremely low energy neutrons, combined with its flexibility and strength, make this metal useful for the construction of thin windows for UCN detectors.

Before the UCN cross section of titanium was determined, it was necessary to obtain an estimate of the number of the UCN transmitted down the guide tube. It was observed that this number, and indeed the velocity spectrum itself are sensitive to the degree of specularly

of the guide tube. From a Monte Carlo simulation the specularity of the guide tube was found to be about 80%. This simulation also gave useful information on the effect of bends on VCN. It was learned that a short connecting section between two bends will filter out VCN more effectively than a longer one. This effect is due to the bunching of VCN near the bottom of the first bend which would result in their striking the second bend surface at an attitude exceeding the critical angle given by equation 2.

To increase the counting rate it is recommended that the guide tube be electropolished in order to decrease the effects of pores and pits. If possible, the converter should be placed deeper in the thermal column as this would also increase the production of UCN.

To minimize the effect of background thermal neutrons, the entire chopper-detector assembly should be shielded using blocks of borinated paraffin.

Table 1

Material	Effective Potential	Theoretical loss factor
	Units of $10^{-3}$ eV	$f = (W/V) \times 10^4$
Ni	27.0	2.5
Be	25.0	0.1 (300°K)
C	18.0	0.1
Cu	17.0	3.1
Mg	6.1	0.2
Al	5.6	0.5
Polythene	-1.1	-
Water	-1.1	-

Table 2

<u>LENGTH OF LINER (L)</u>	<u>SPECZ</u>	<u>X=TPL/ND</u>	<u>F=X/(80-L)</u>
------------------------------------	--------------	-----------------	-------------------

## UCN V=5.7 meters/sec

0	100	118.0	1.48
10	100	85.9	1.23
20	100	80.0	1.33
0	80	166.0	2.07
10	80	101.9	1.46
20	80	91.0	1.52
0	60	225.0	2.81
10	60	139.0	1.98
20	60	101.9	1.70

## VCN V=7.0 meters/sec

10	100	87.3	1.25
10	80	90.5	1.29
10	60	85.6	1.22

## VCN V=9.0 meters/sec

10	80	83.6	1.19
----	----	------	------

## VCN V=12.0 meters/sec

10	80	83.9	1.20
----	----	------	------

Table 3

Channel Area	Velocity Range	Mean Velocity	Titanium Foil Thickness in Mil				
			0.0	0.5	1.0	2.0	4.0
12-14	7.4-6.5 m/sec	6.95 m/sec	828	793	358	355	219
14-16	6.5-5.7 m/sec	6.10 m/sec	1103	966	561	401	209
16-18	5.7-5.2 m/sec	5.45 m/sec	1150	1230	570	340	128

\* Numbers in last column are integrated counts in indicated channel area for various Ti foil thickness.

Table 4

<u>Observed Velocity</u> <u>v in m/sec</u>	<u>Corrected Velocity</u> <u>v' in m/sec</u>	<u>Apparant Mean Free</u> <u>Path in inches (q')</u>	<u>Loss Cross Section</u> <u><math>\sigma</math> in barns</u>	<u>Normalized Loss</u> <u>Cross Section <math>\sigma'/2200</math></u>
6.95	7.58	0.00381 $\pm$ .0008	1832 $\pm$ 450	6.70 $\pm$ 1.3
6.10	6.8	0.00317 $\pm$ .0006	2202 $\pm$ 490	7.34 $\pm$ 1.1
5.45	6.26	0.00235 $\pm$ .0004	2971 $\pm$ 600	9.18 $\pm$ 2.3


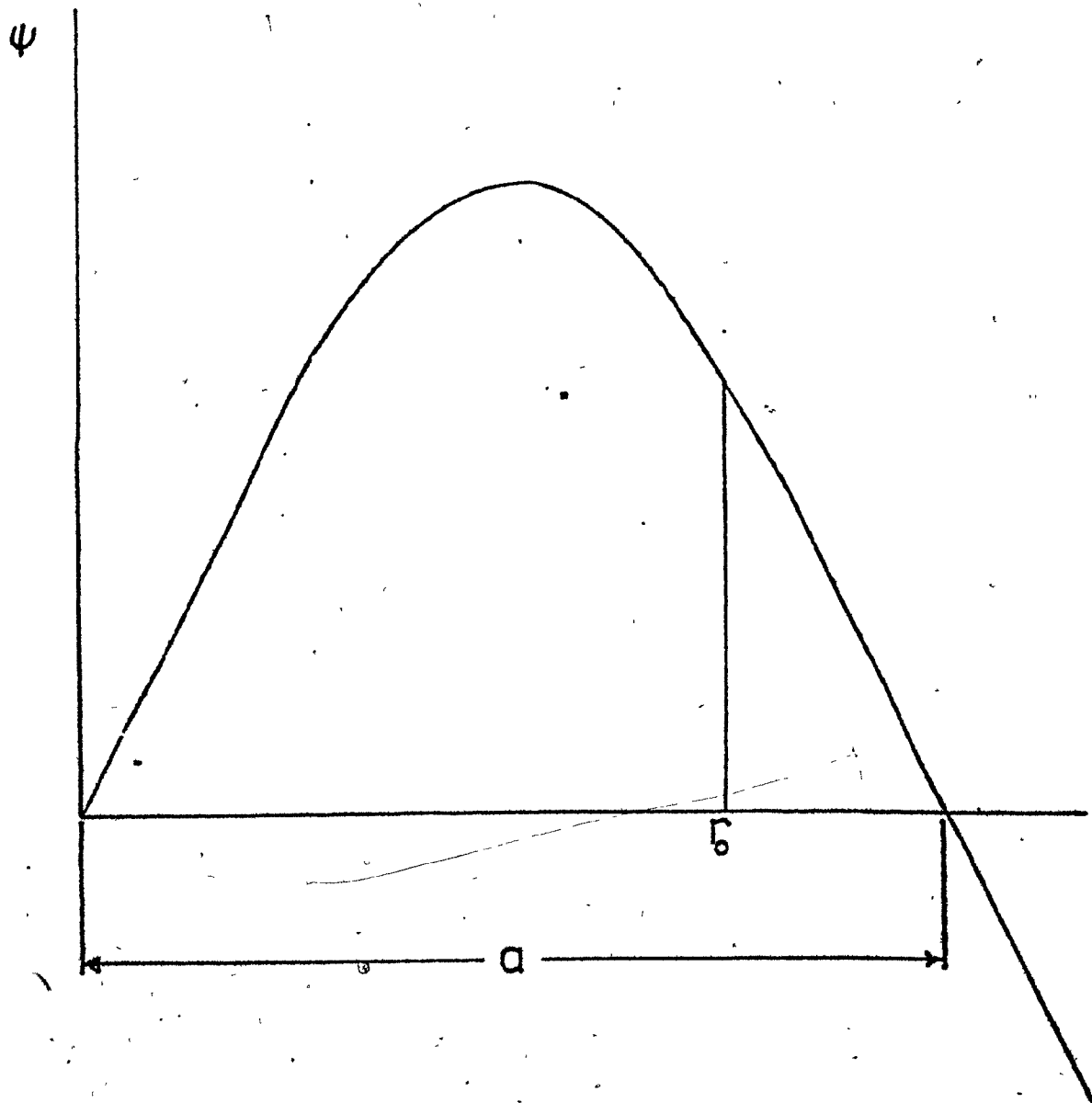


Fig 1. Illustration of the physical meaning of a positive scattering length. The wave function is plotted against radial distance. The scattering length is the extrapolated intercept of the wave function on the  $r$  axis.








Fig 2. Illustration of the physical meaning of a negative scattering length. The wave function is plotted against radial distance. The scattering length is the extrapolated intercept of the wave function on the  $r$  axis.

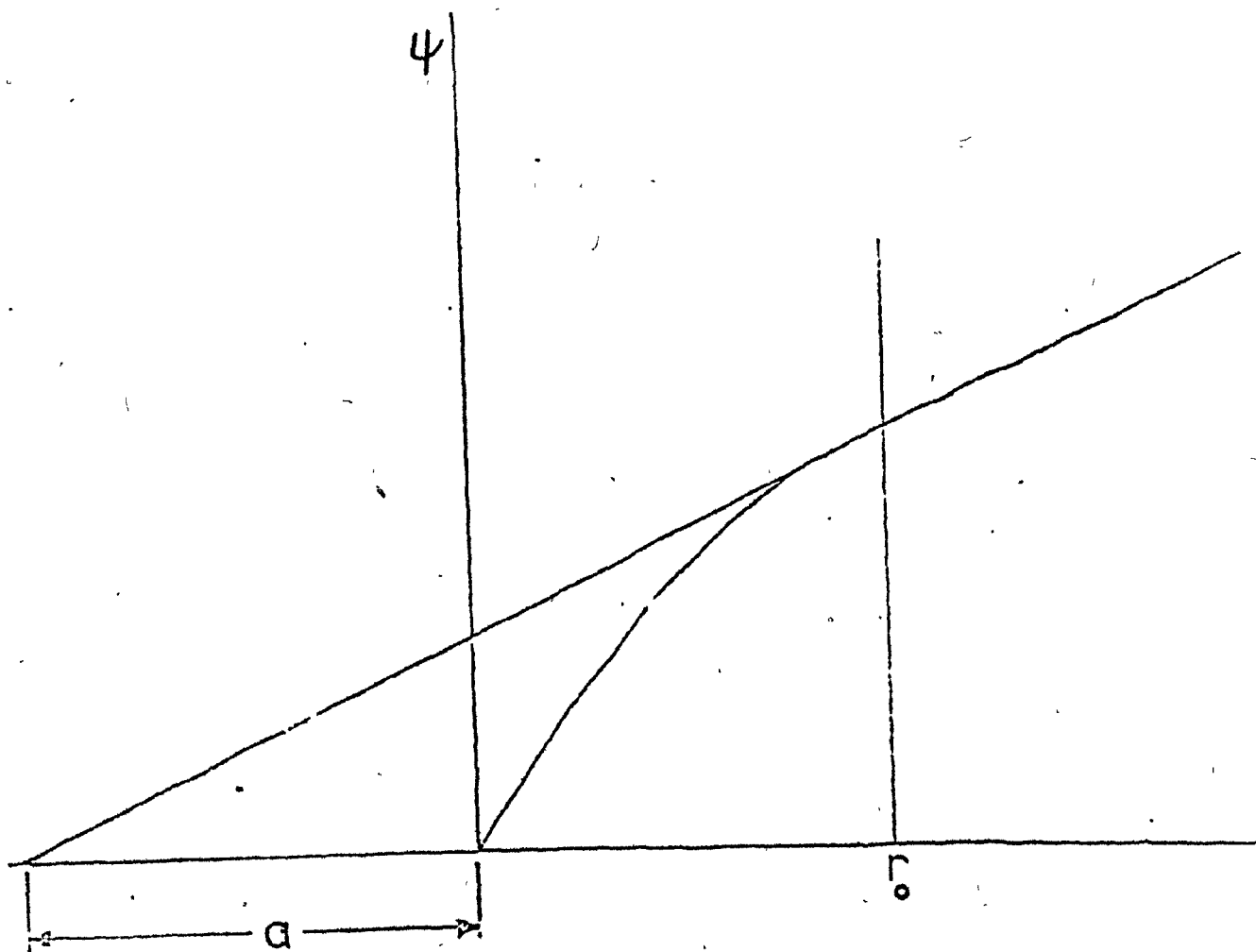
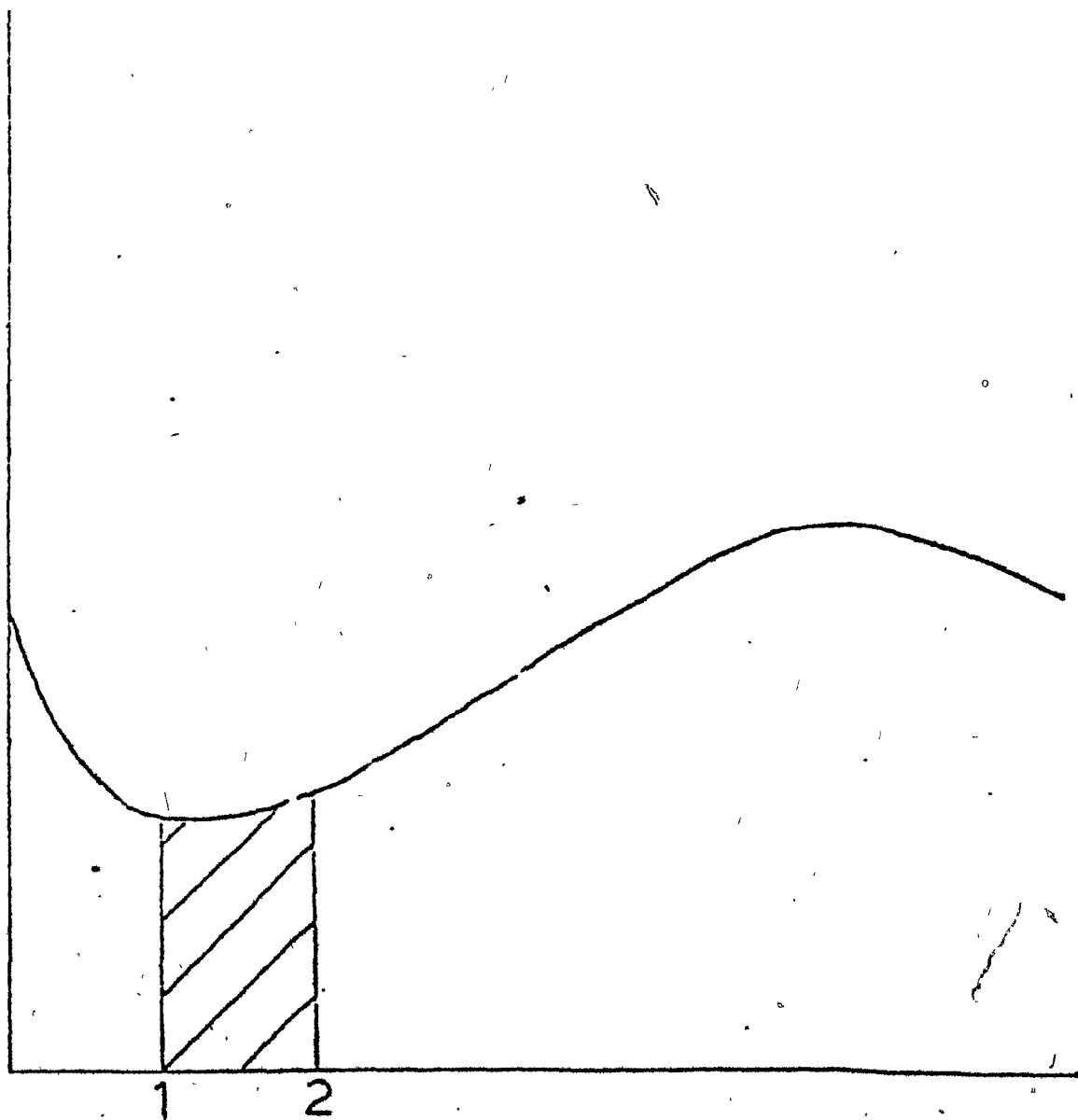


Fig 3. Illustration of the spectrum obtained from the detector when placed next to an Am-Be neutron source. The discriminator was set to fire above the noise. The shaded area 1-2 corresponds to the quiescent region.

COUNTS



CHANNEL NUMBER

Fig 4. Illustration of the effect of polythene liner length on UCN count rate. The large background can be reduced by using more shielding. The background shown here was measured in different runs and its average is 2800 counts per 800 seconds.

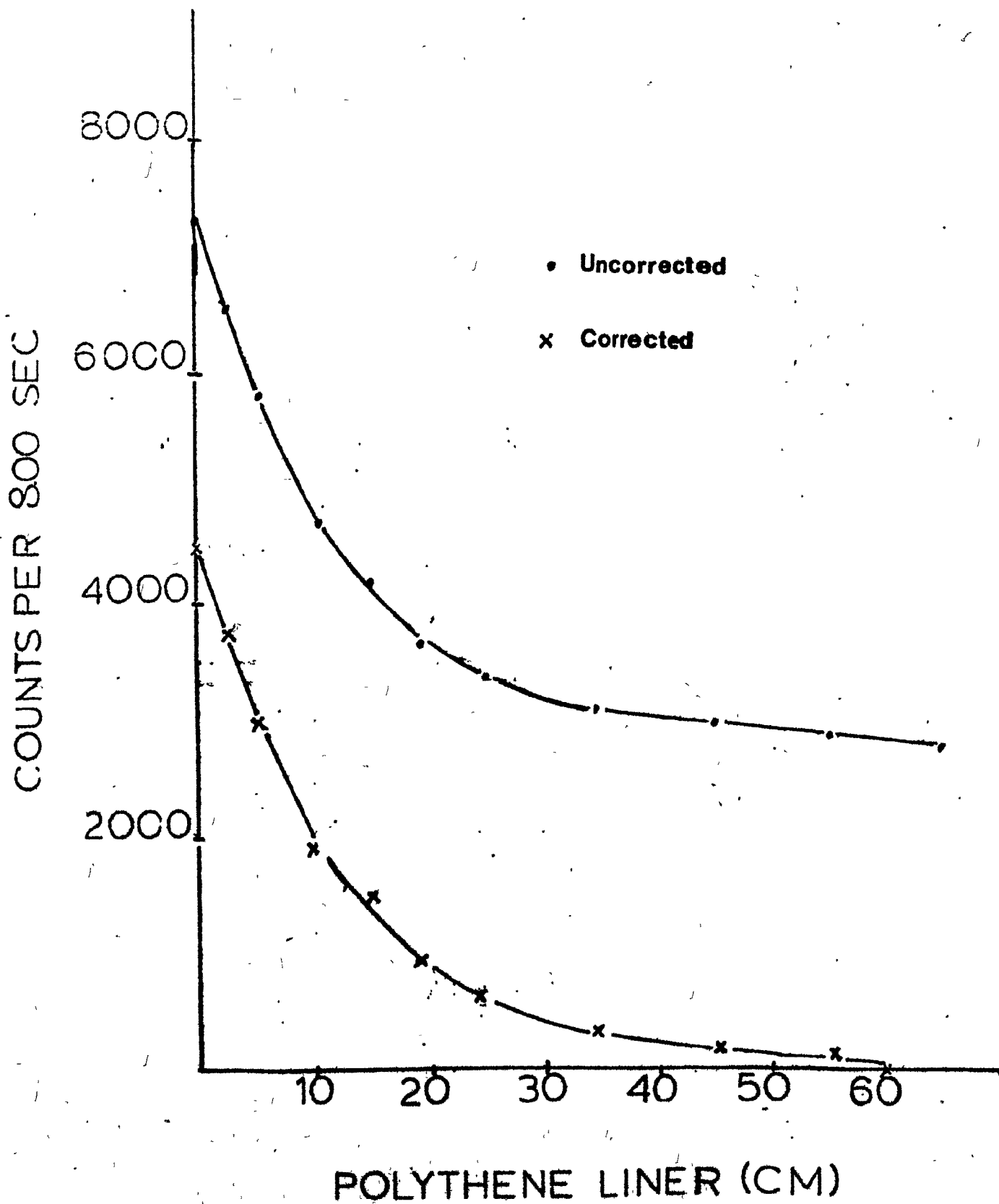


Fig 5. Illustration of data in a typical time of flight run. All counts below the line are considered as noise. Note that the line is not horizontal as is expected, but slightly skewed. This is due to a variable background noise confirmed in separate runs. In the analysis the first peak corresponding to noise was ignored.

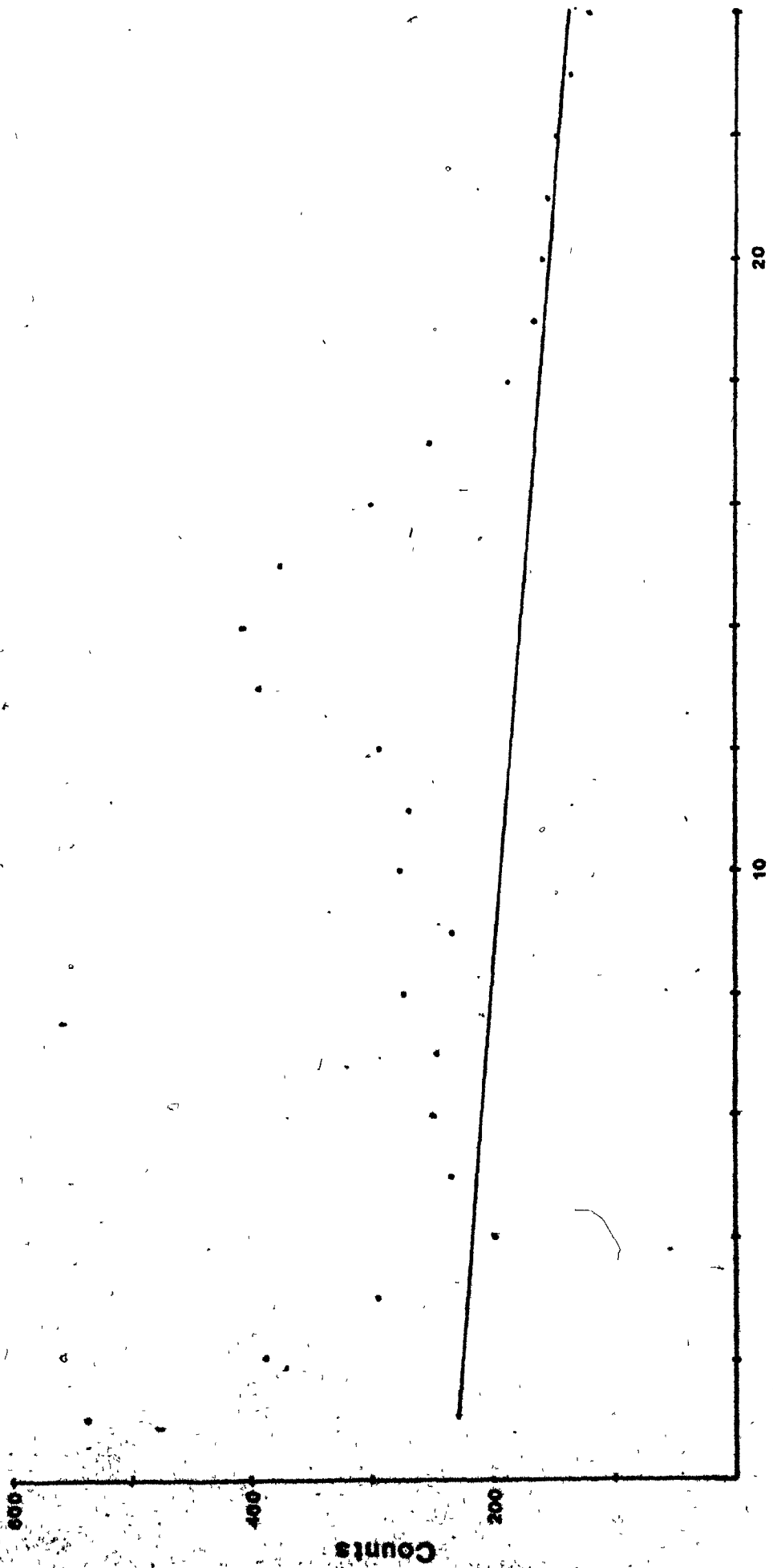
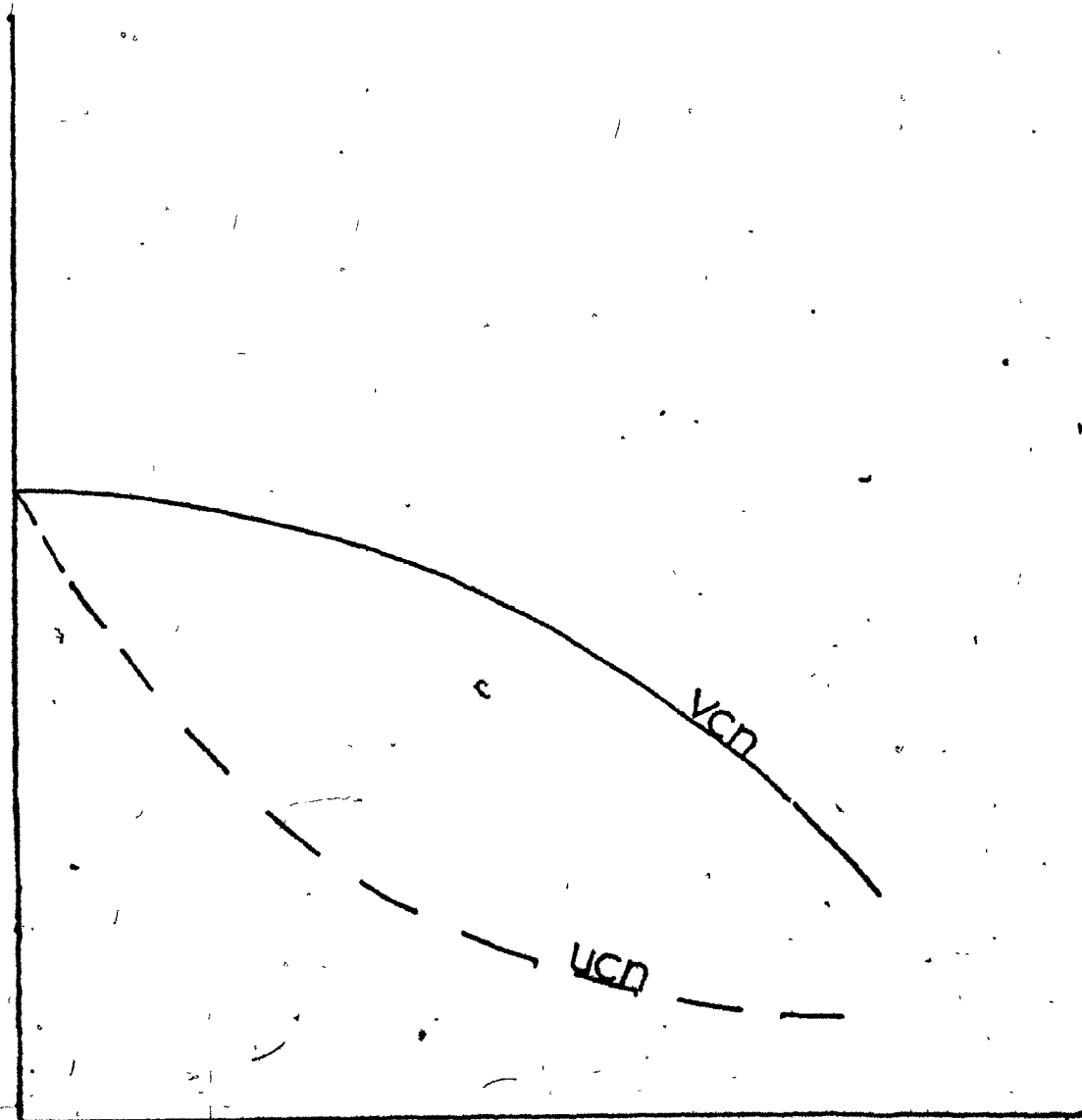




Fig 6. Illustration of the expected variation in the number of VCN and UCN striking the central region of the detector as a function of polythene liner length.

COUNTS



LENGTH OF LINER

Fig. 7. Illustration of the effect of specularity on counting rate for UCN predicted by a Monte Carlo simulation.

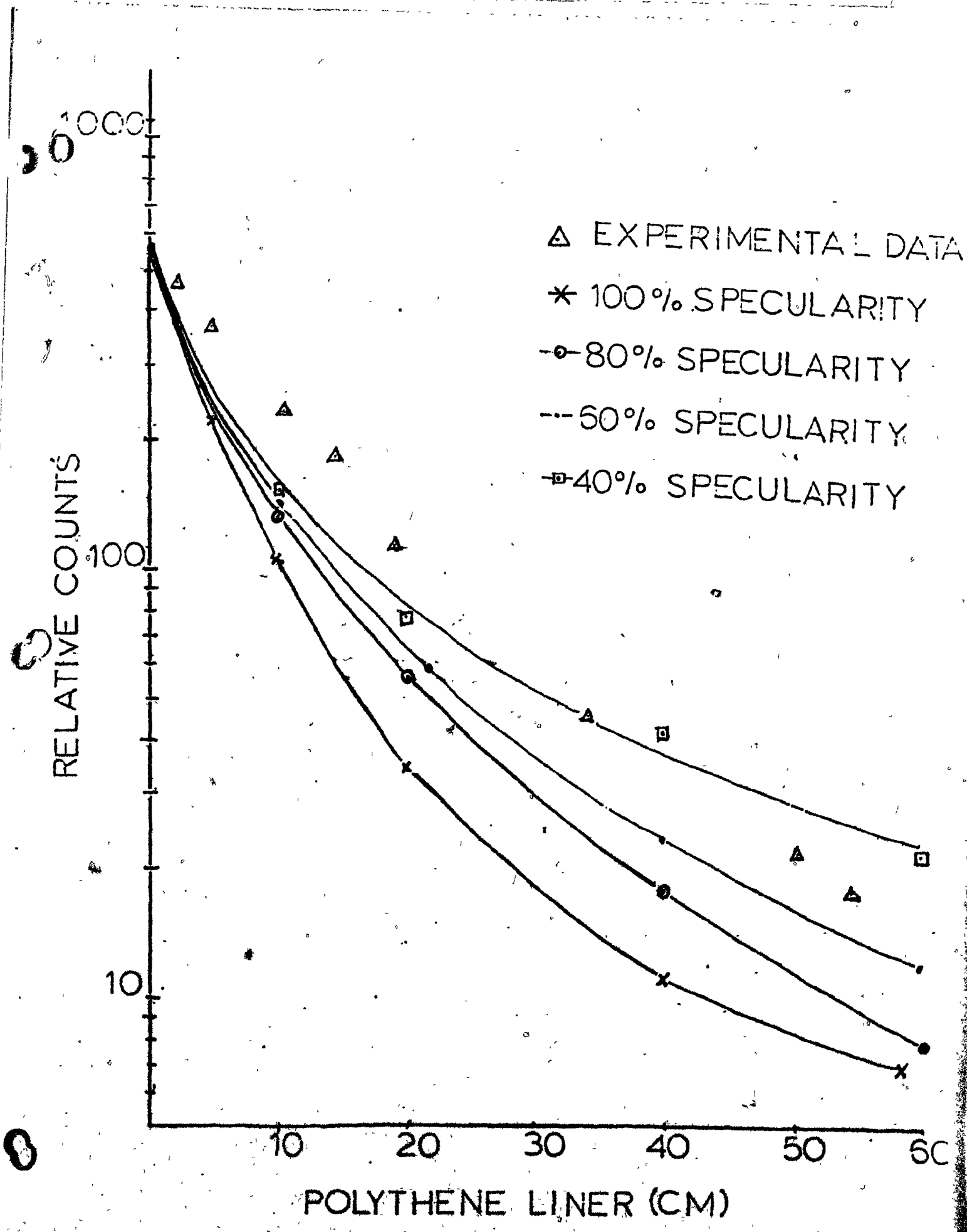


Fig 8. Illustration of the effect of various lengths of tubing between bends. A short section is predicted to filter out VCN more effectively than a longer one.

COUNTS

100

10

5

10

15

20

VELOCITY (M/SEC)

- 10 CM
- x 70 CM
- Δ 30 CM
- ▽ 100 CM

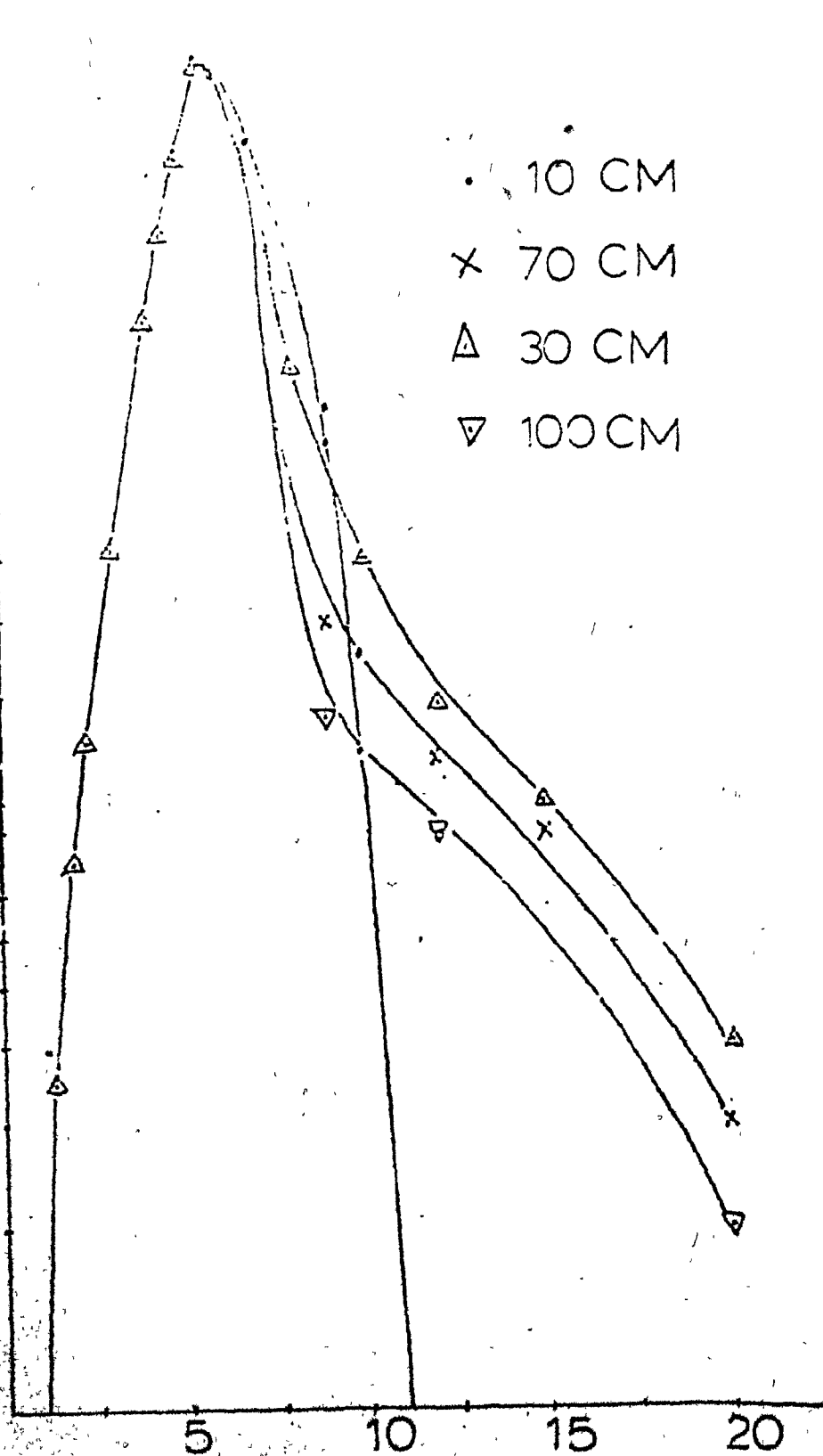


Fig 9. Velocity spectrum shown as a time of flight spectrum  
for a 100 cm between bends.

-x- RESOLUTION FOLDED

-- RESOLUTION NOT FOLDED

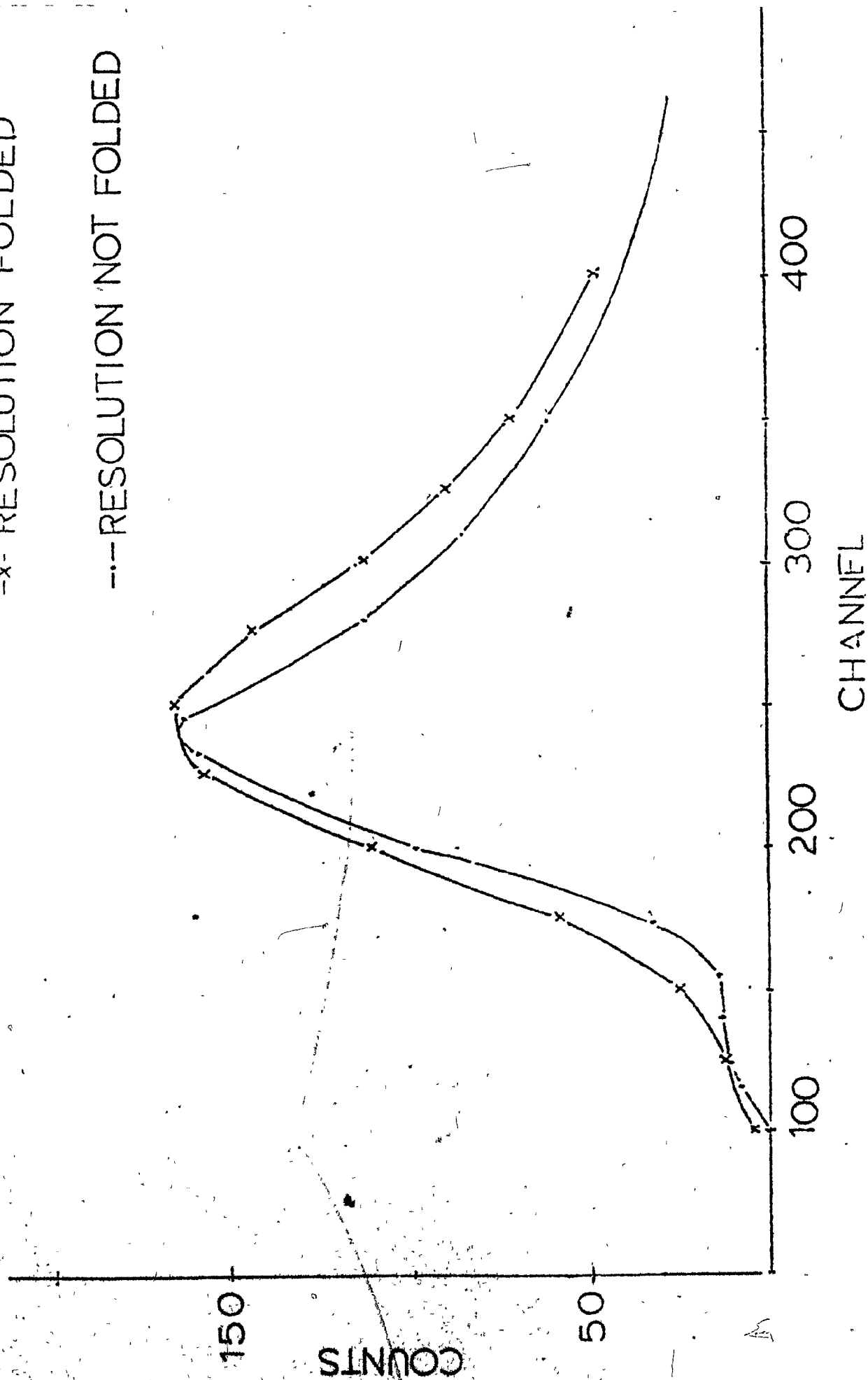




Fig. 10 Illustration of the effects of specularity on pure UCN, combinations of UCN and VCN, and on VCN as predicted by a Monte Carlo simulation. The unrefrenced points are experimental.

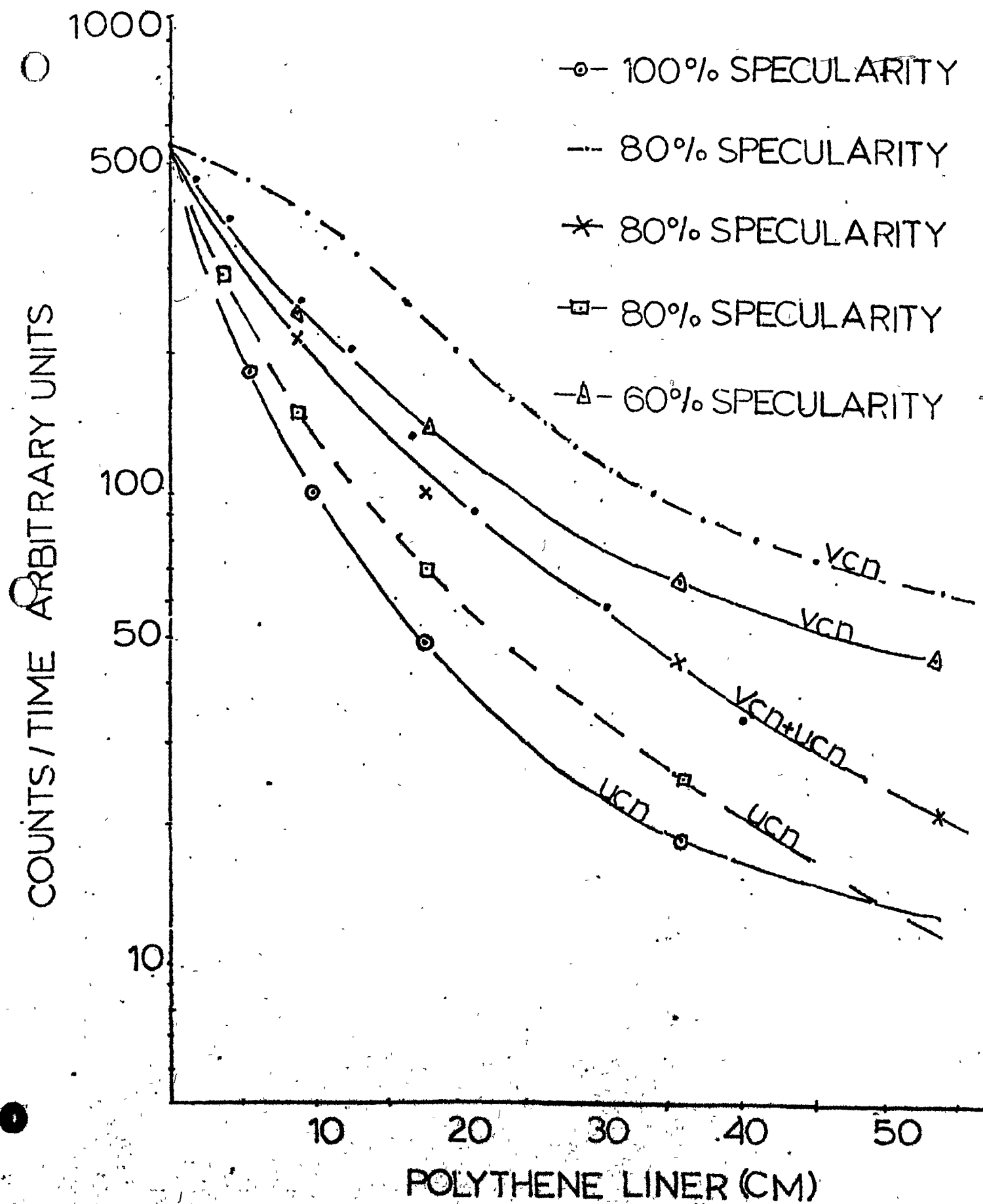


Fig. 11. Plot of velocity against channel number reveals a linear region extending from channels 12-22. Three sections in this region were used to estimate the cross section.

VELOCITY (M/SEC)

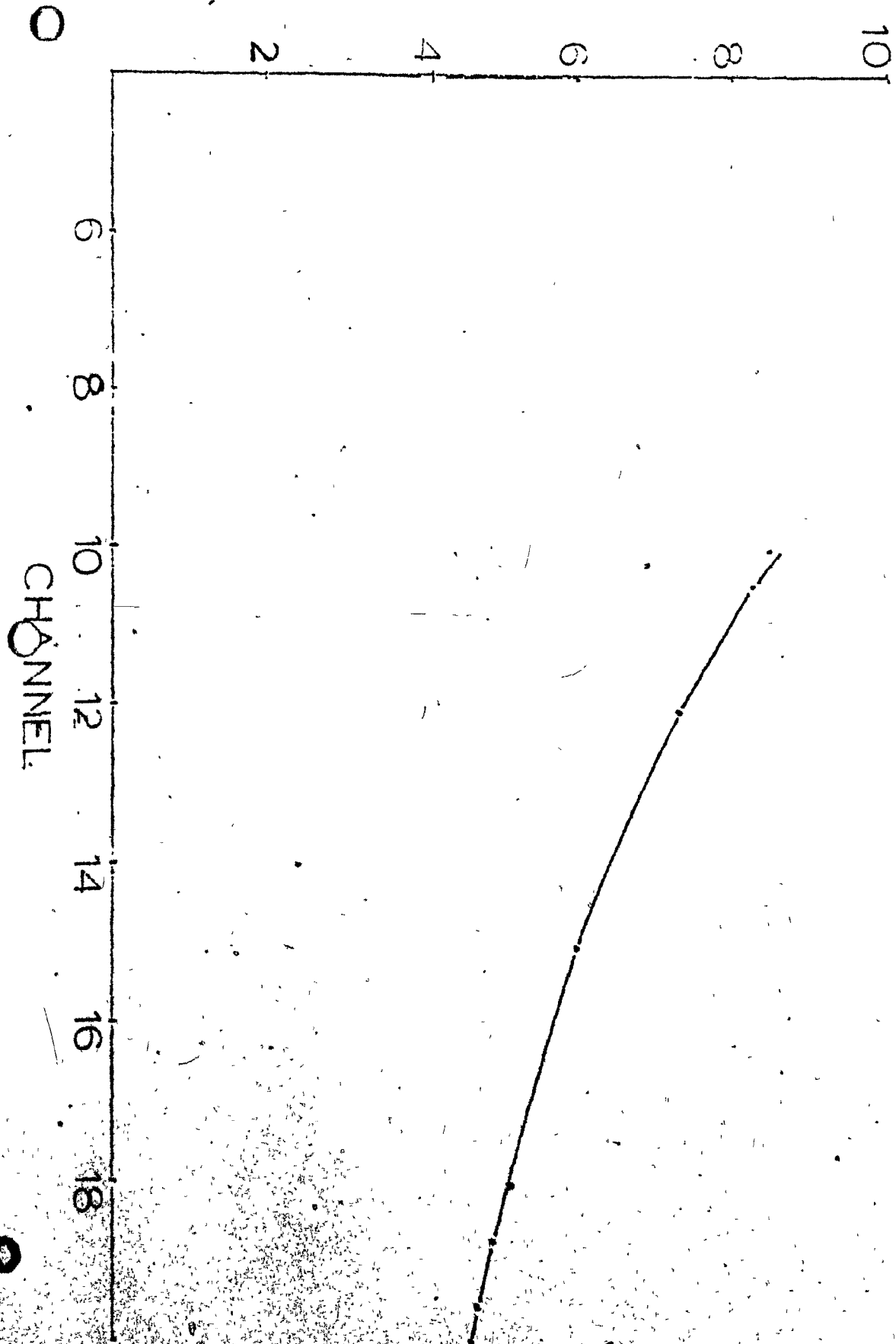
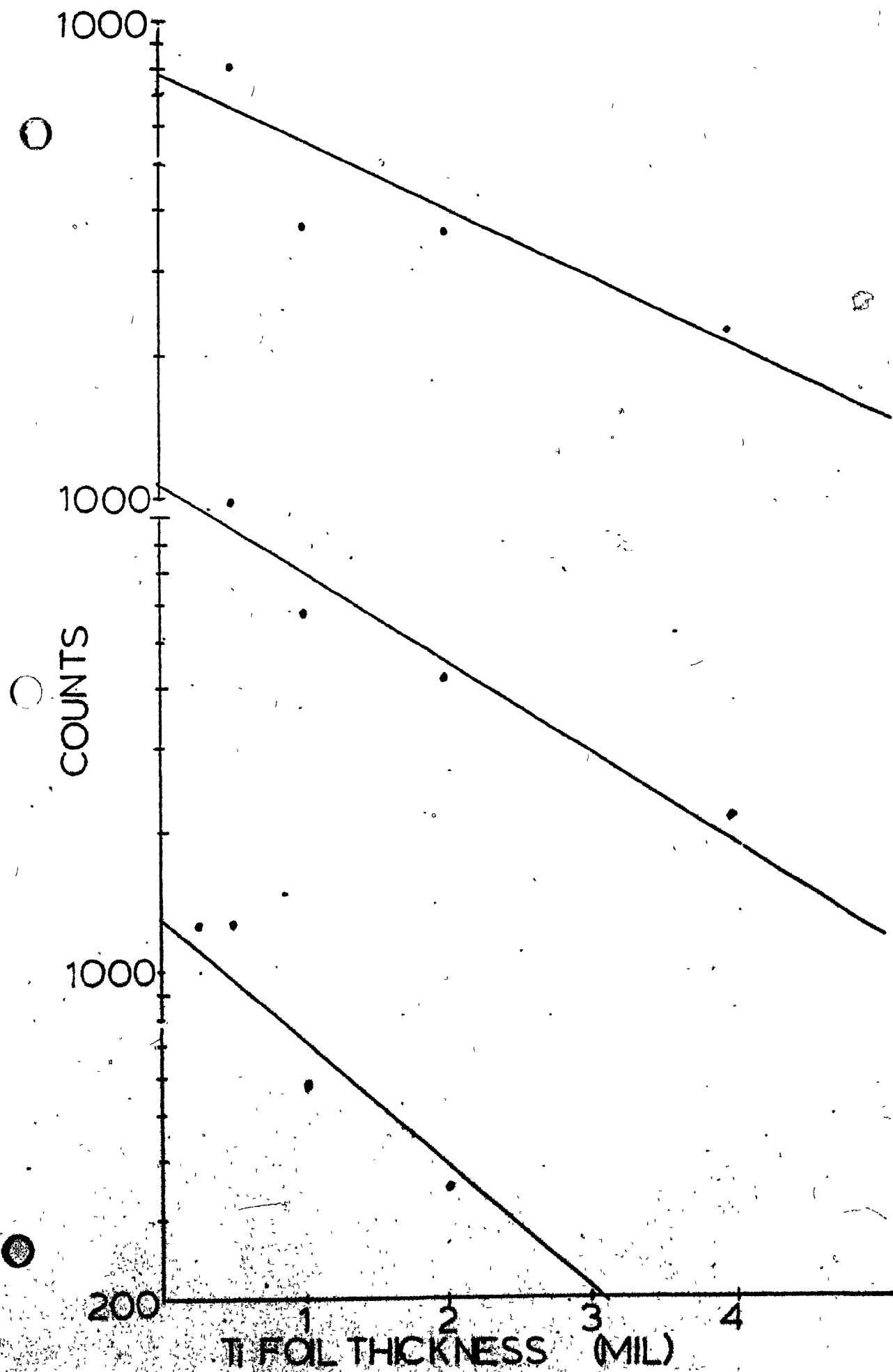


Fig 12. Plot of integrated counts in the regions 12-14, 14-16, 16-18 against titanium foil thickness.





The figure is a plot with a vertical y-axis and a horizontal x-axis. A dashed line starts from the y-axis and extends diagonally downwards to the right. Several data points are plotted, mostly following the path of the dashed line. Three points are marked with open circles, while the others are small dots. The points are distributed across the plot, with a higher density at lower values on both axes.

Fig 13. Plot of loss cross section as a function of velocity.

Three points are experimental. The rest are from the Barn Book.

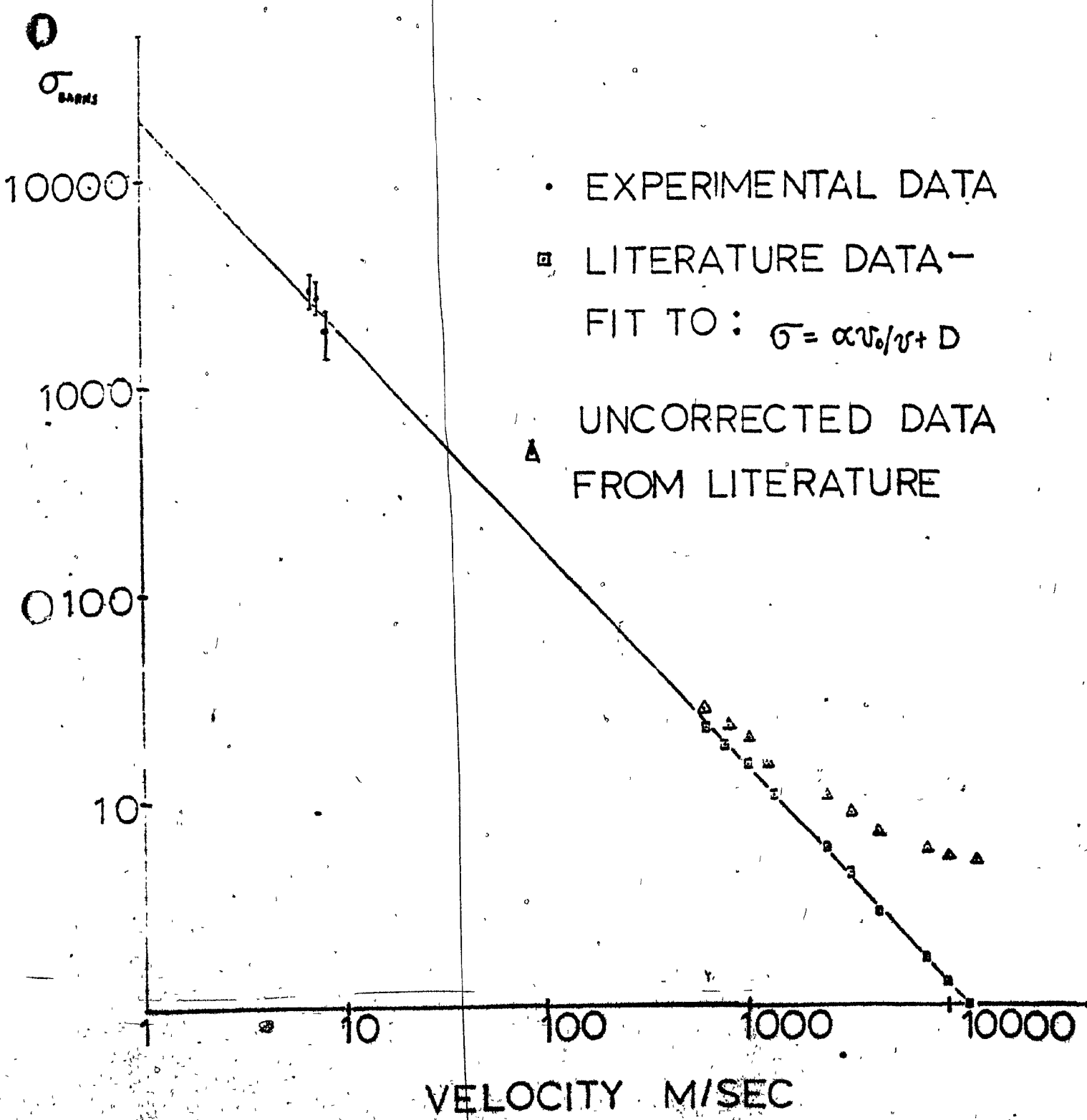




Fig 14. Form of ideal potential. The potential here is plotted as a function of distance.

0

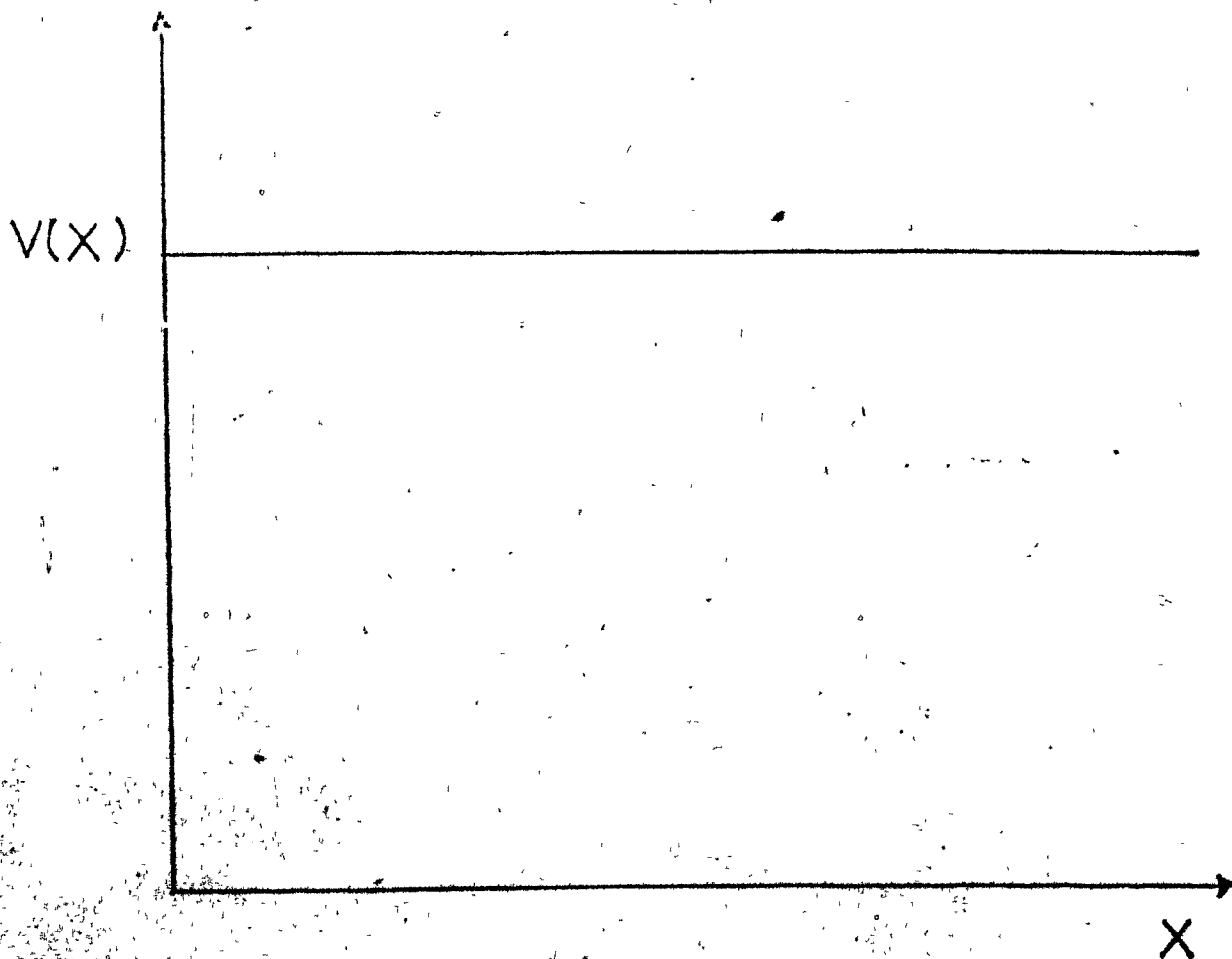


Fig 15. Form of actual potential. The potential here is plotted as a function of distance.

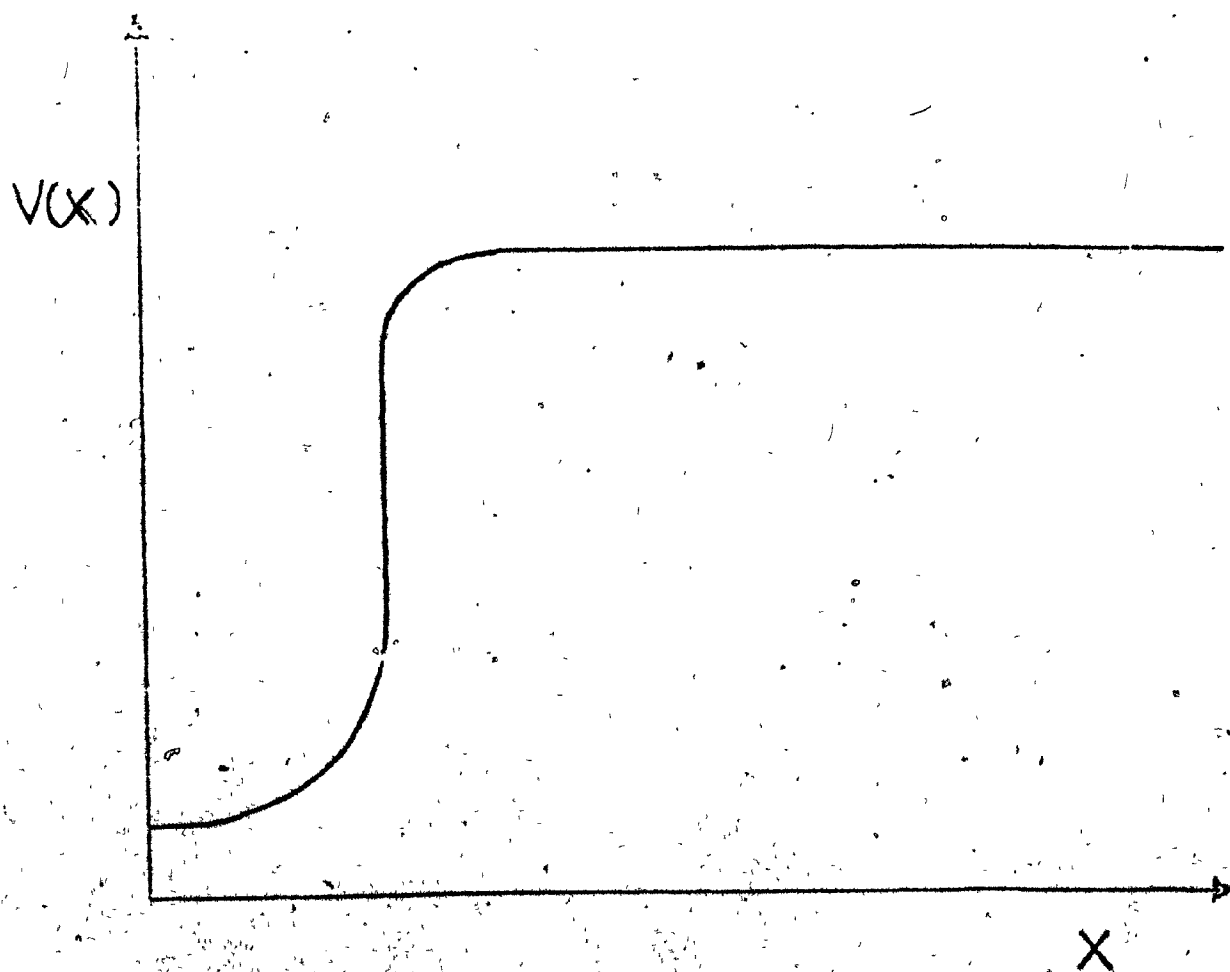


Fig. 16. Plot of  $F$  against velocity. Values of  $F$  were obtained from a Monte Carlo simulation, keeping the polythene liner length fixed at 10 cms, and the specularity constant at 50%.

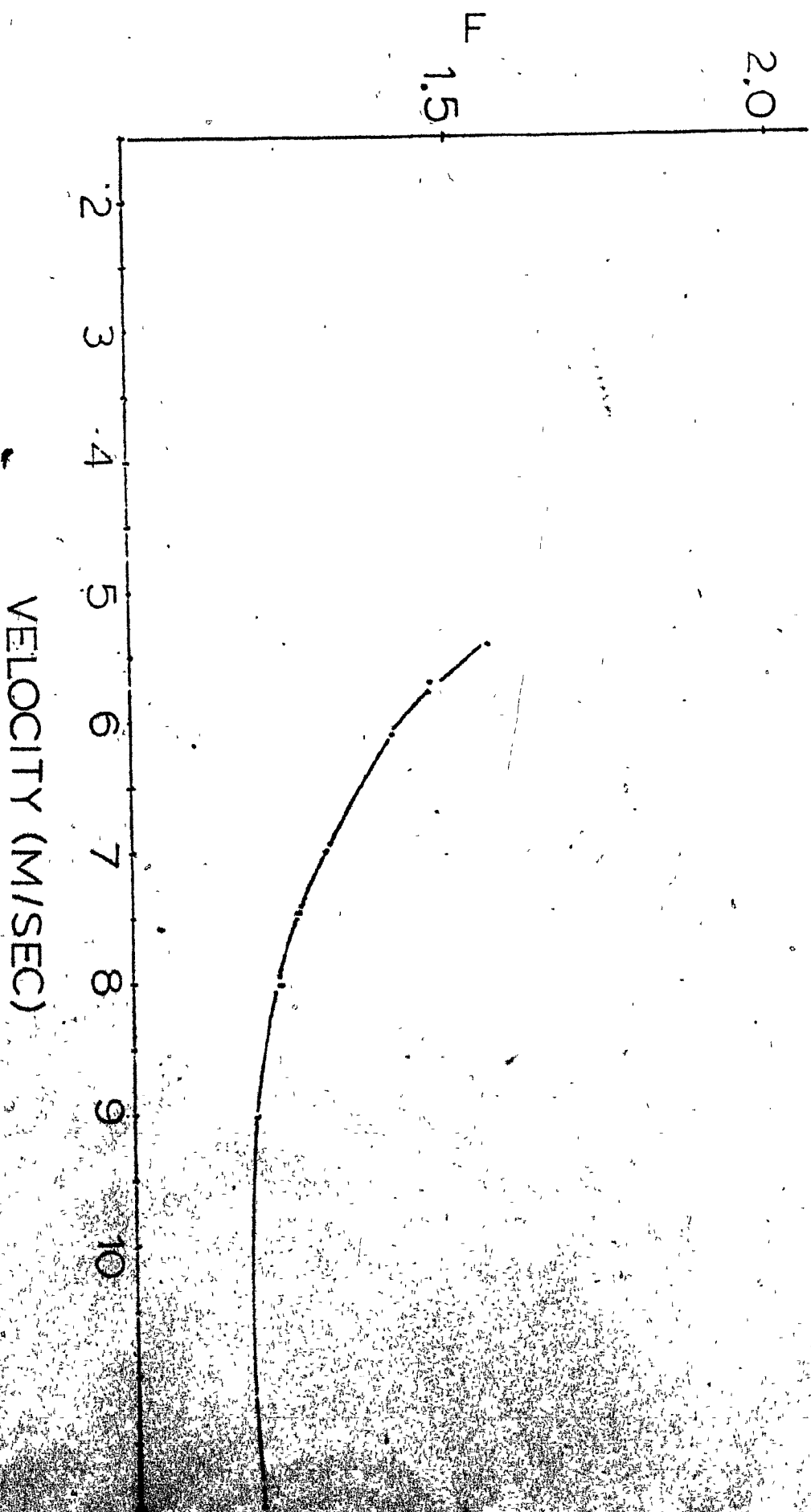


Fig.17. Plot of counts as a function of various thickness of titanium foil. The regions extending from channels 12-18 were used in calculating the loss cross section.

in  
 0  
 .0005  
 .001  
 .002  
 .004

-A-  
 -O-  
 -E-  
 -V-

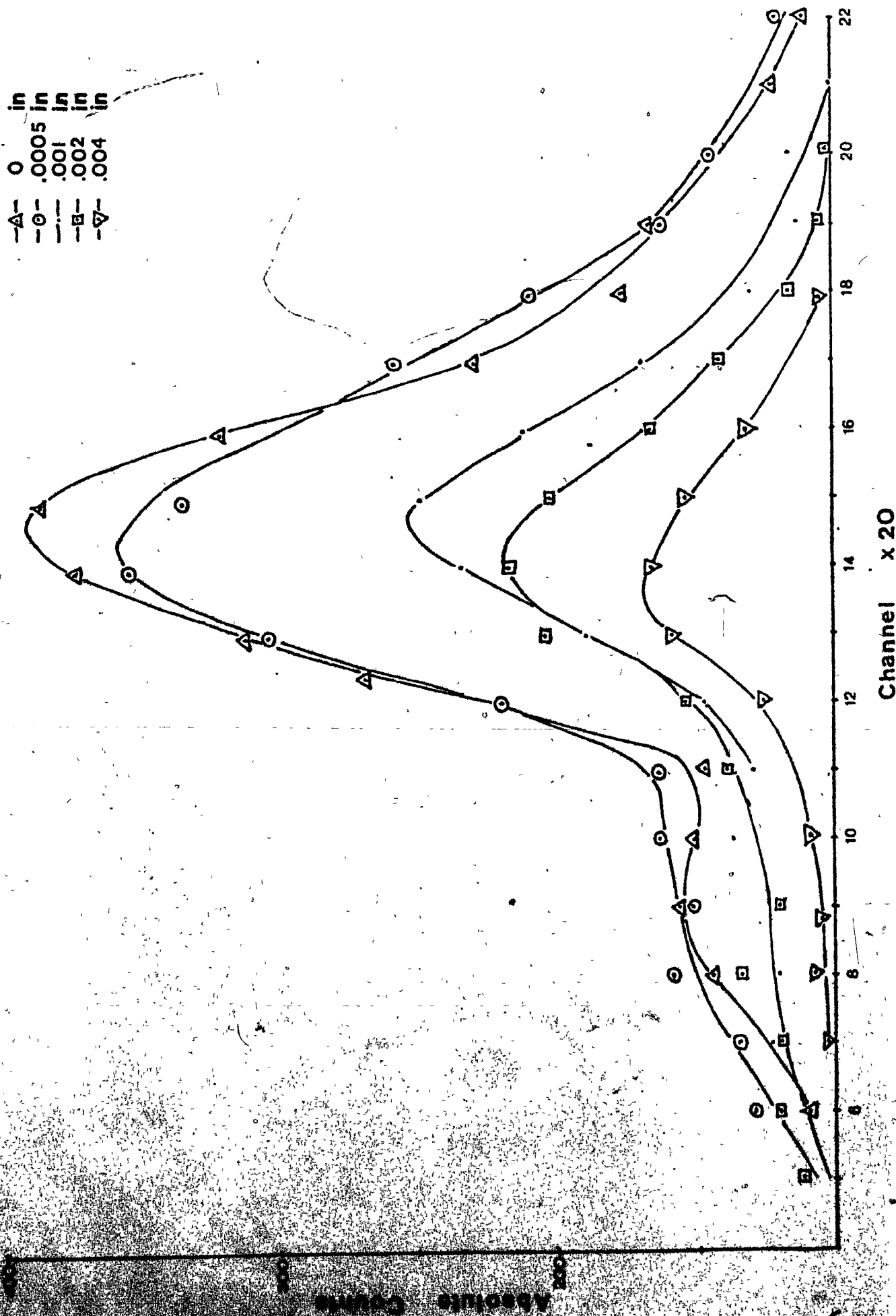
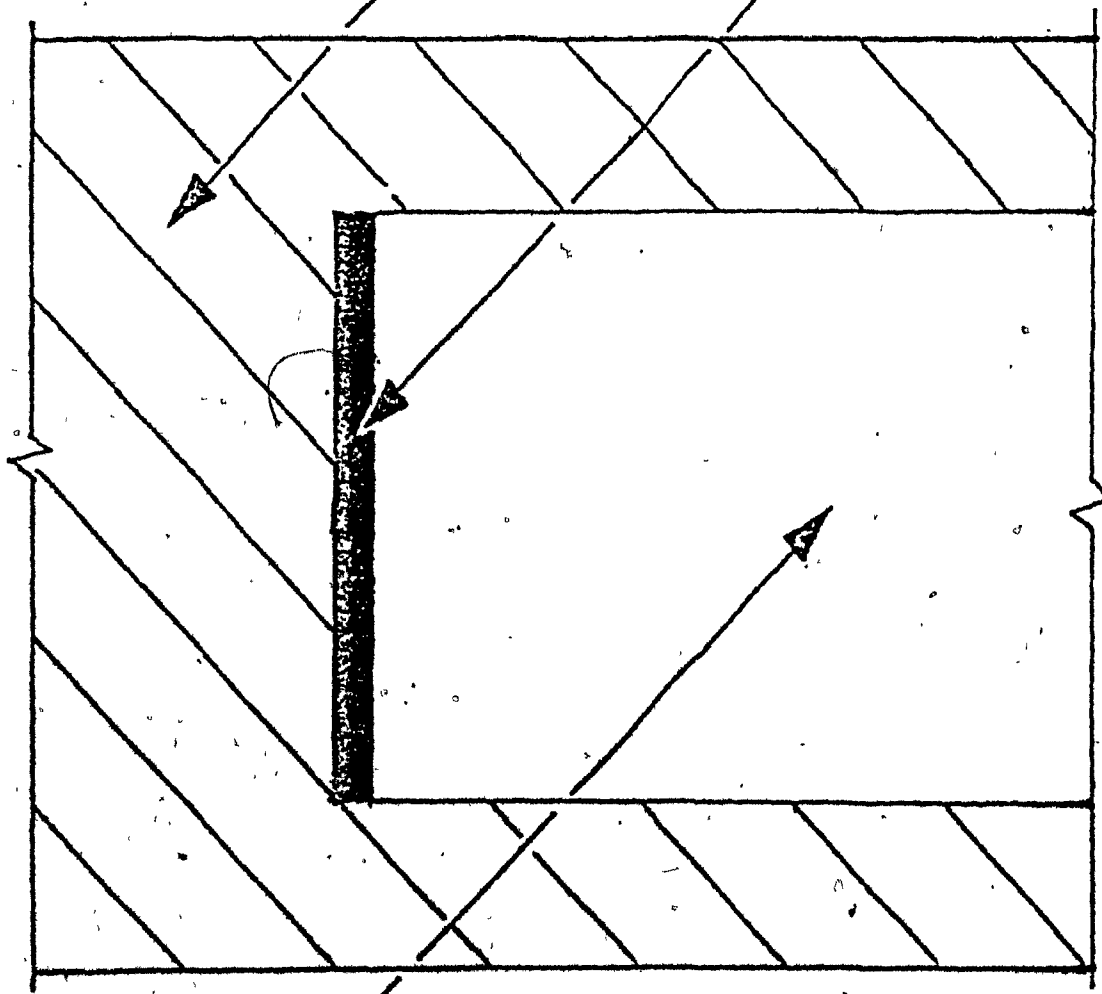




Diagram 1. Illustration of converter. The converter is a polythene disc attached to the end of a copper tube. By cooling the disc to liquid nitrogen temperature, the UCN production rate is increased. The copper tube is evacuated to minimize the interaction of UCN with air.

Thermal  
Column

Polythene  
Converter



2" Diameter Copper Tube

Diagram 2. Illustration of geometry. All neutrons outside the UCN or VCN energy range will go straight through the first elbow and into an absorbing medium. UCN and VCN will be channeled by the conduits into the guide tubes leading to the chopper.

3" Diameter  
Copper Tube

To Chopper →

Thermal  
Column

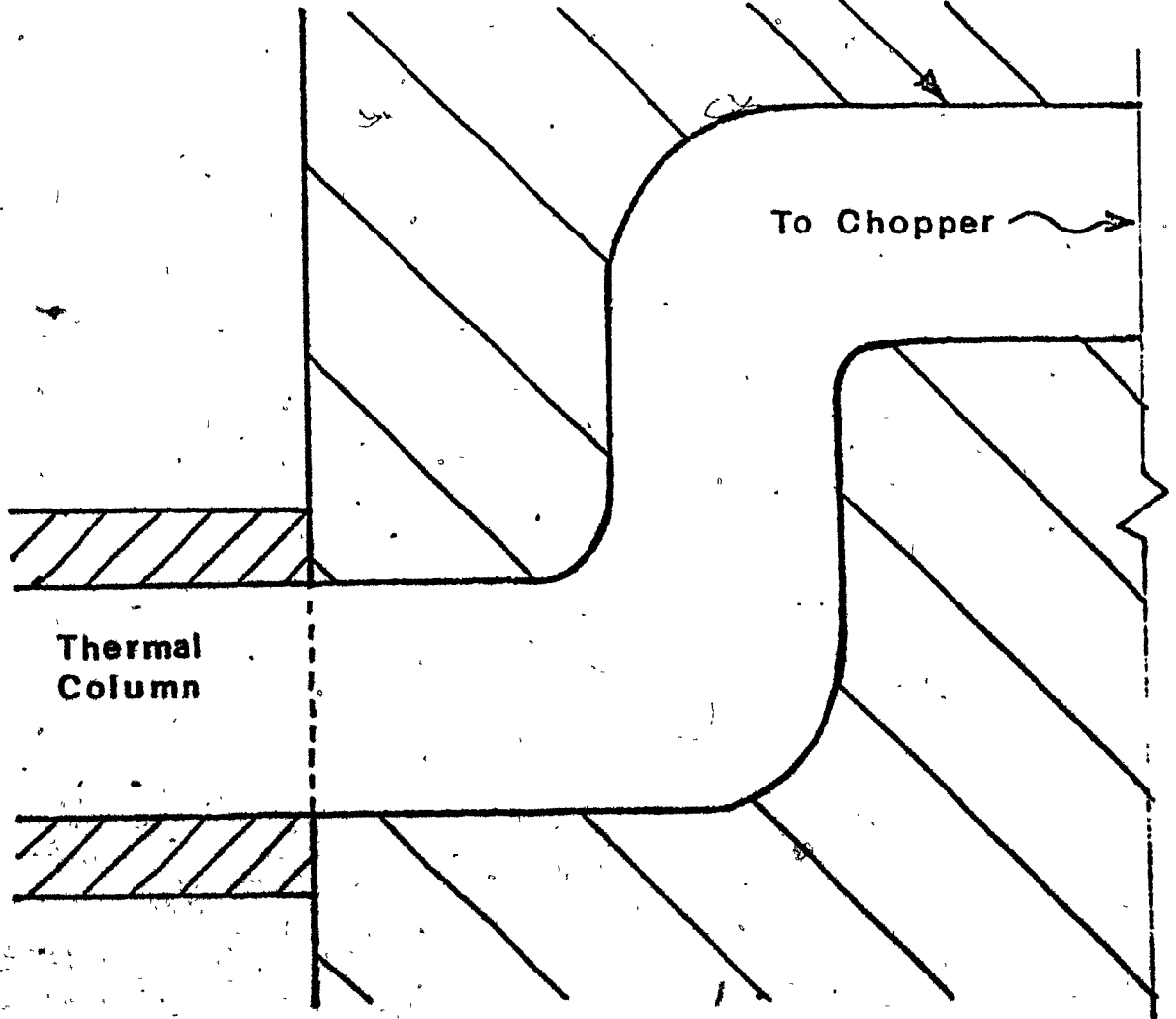


Diagram 3. Illustration of chopper assembly. The detector is located 50 cms from the chopper. The disc is the circular object to the right of the chopper. The small off centered hole allows light through only when the chopper is on. Light reaching the photocell produces the timing signal.

Chopper

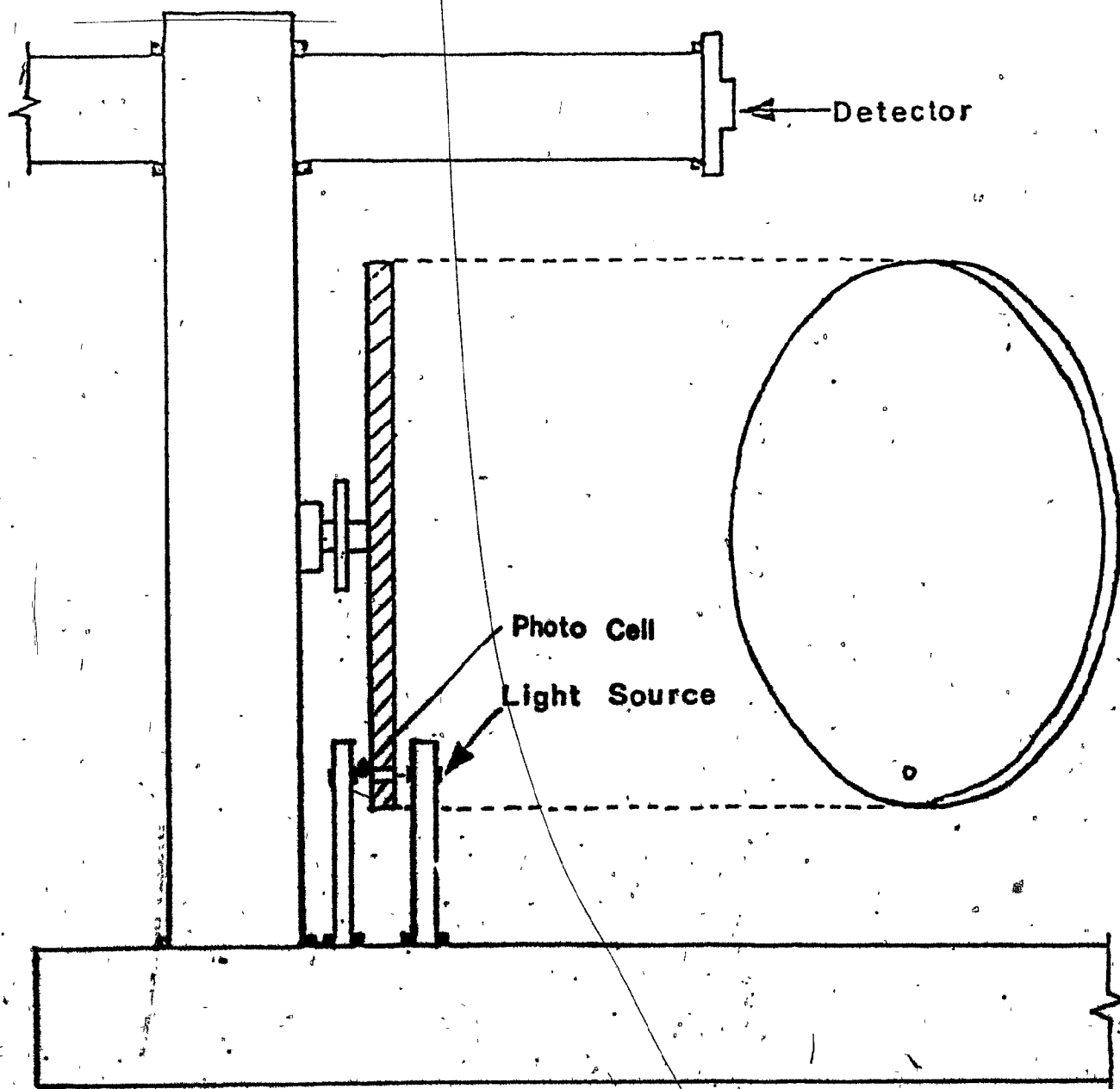


Diagram 4. Illustration of timing circuitry. A discriminator was used to convert the analogue signal from the amplifier to a pulse which triggered the MCS.

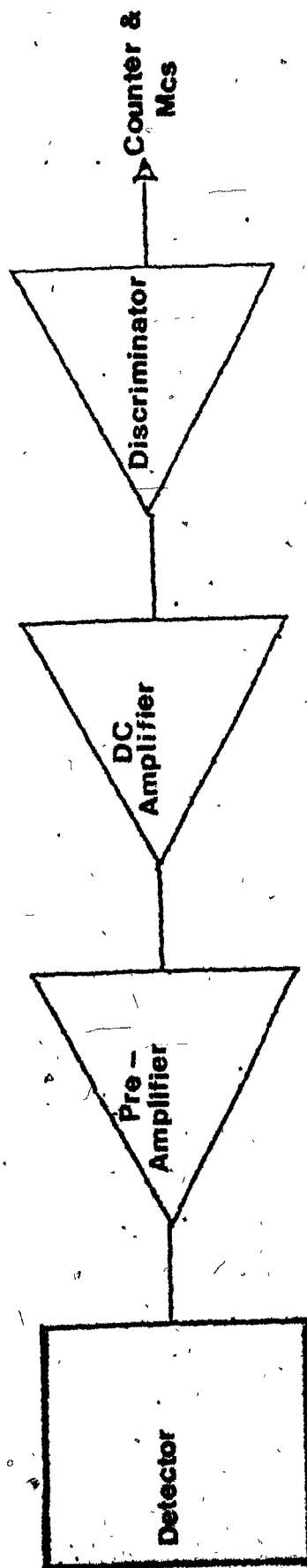
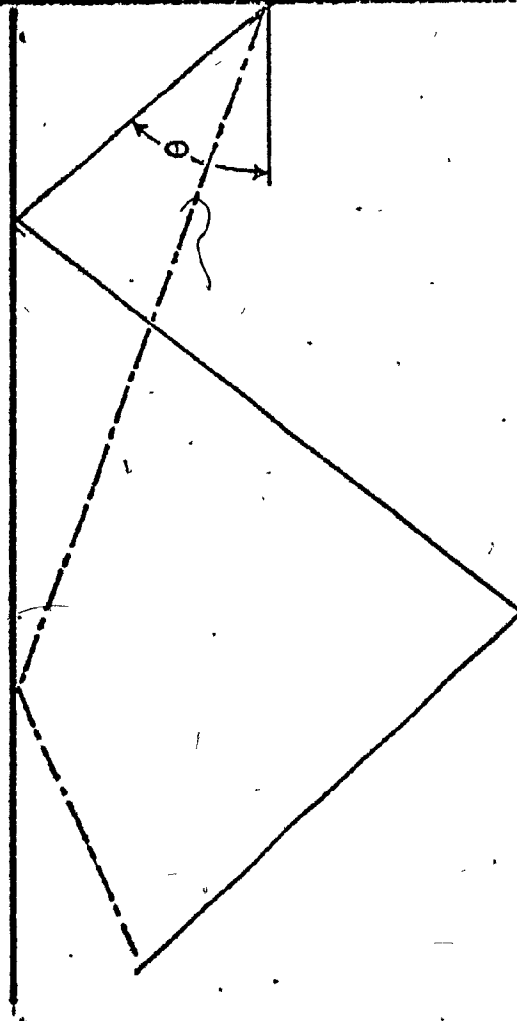
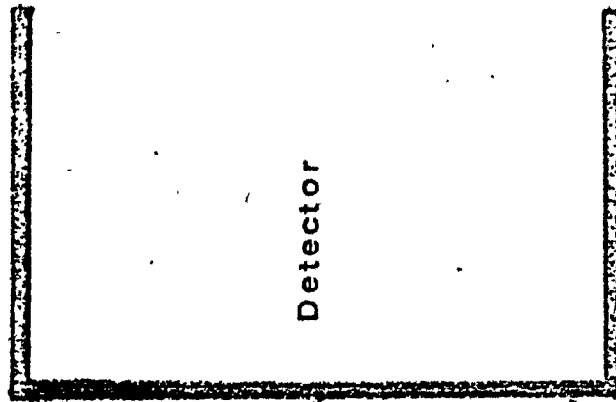




Diagram 5. Illustration of typical UCN and VCN trajectories.

The solid line is a UCN path segment. The variable  $F$  found from the Monte Carlo simulation equals  $\sec \theta$ .



Bibliography

- 1) Antonov, A.V., Isakov, A.I., Kasarnoviskii, M.V. and Solodilov, V.E., (1969), JETP Letts 10, 241-244.
- 2) Blatt, J.M. and Weiskopf, V.F. (1952), Theoretical Nuclear Physics, John Wiley, New York.
- 3) Egelstaff, P.A. and Poole, M.J. (1969), Experimental Neutron Thermalization, Pergamon, Oxford.
- 4) Fermi, E. (1936), Ricerca Scientifica, 7, 13-52.
- 5) Fermi, E. (1950), Nuclear Physics, compiled by Orear, J., Rosenfeld, A.H. and Schluter, R.A., Revised Edition, University of Chicago press, Chicago.
- 6) Fermi, E. and Zinn, W.N. (1946), Phys. Rev. 70, 103.
- 7) Fermi, E. and Marshall, L. (1947), Phys. Rev. 71, 666-667.
- 8) Goldberger, M.L. and Seitz, F. (1947), phys. 71, 294-310.
- 9) Golub, R. (1972), Physics Letters 38A, 177-178.
- 10) Ignatovich, V.K., (1972), Joint Institute of Nuclear Research, Dubna, USSR, Communication P4-6653.

- 11) Glasstone, S. and Edlund, L. M. (1952), The Elements of Nuclear Reactor Theory, Van Nostrand.
- 12) Hughes, D. J., (1954), Neutron Optics, Interscience Tracts on Physics and Astronomy.
- 13) Steyerl, A. (1977), Very Low Energy Neutrons, Springer Tracts Vol. 80 p 57.
- 14) Schmatz et. al. (1974), Journal of Applied Crystallography, Vol 1 p 96.
- 15) Englemann et. al., Zeitschrift fur Physik B. (1979), Vol. 35, p 345.
- 16) Luschikov, V.I., Pokotilovsky, Y.N., Strelkov, A.V. and Shapiro, F.L. (1958), Joint Institute of Nuclear Research, Dubna, USSR, preprint P3-4127.
- 17) Binder, K. Phys. Stat. Sol., Vol 41, p 767, (1970). Also quoted in Steyerl, A, (1977).
- 18) Golub, R., Pendlebury, J. M., Ultra-Cold Neutrons, Reports on Progress in Physics.

## IMPURITIES IN TITANIUM FOIL

Element	Concentration ppmw
Fe	$1 \times 10^2$
K	$3 \times 10^1$
Mn	2
Co	<1
Se	9
Al	$2 \times 10^1$
Cl	$3 \times 10^1$
Te	$8 \times 10^1$
Sn	$1 \times 10^2$
Mg	$1 \times 10^1$
As	2
Sb	2